Article

Turning-On of Coumarin Phosphorescence in Acetylacetonato Platinum Complexes of Cyclometalated Pyridyl-Substituted Coumarins

Andrej Jackel, Michael Linseis, Christian Häge, and Rainer F. Winter *

Fachbereich Chemie der Universität Konstanz, Universitätsstraße 10, D-78457 Konstanz, Germany;
E-Mails: andrej.jackel@uni-konstanz.de (A.J.), michael.linseis@uni-konstanz.de (M.L.);
christian.haege@uni-konstanz.de (C.H.)

Academic Editors: Axel Klein and Elena Lalinde

* Author to whom correspondence should be addressed; E-Mail: rainer.winter@uni-konstanz.de;
Tel.: +49 7531 885355; Fax: +49 7531 883136.

Abstract: Two pyridine-functionalized coumarins differing with respect to the site of pyridine attachment to the coumarin dye (3 in **L1** or 7 in **L2**) and with respect to the presence (**L1**) or absence (**L2**) of a peripheral NMe_2 donor were prepared and used as cyclometalating ligands towards the Pt(acac) fragment. X-ray crystal structures of complexes **1** and **2** show strong intermolecular interactions by π-stacking and short Pt···Pt or C-H···O hydrogen bonding that result in the formation of sheetlike packing patterns. The NMe_2 donor substituent has a profound influence on the absorption and emission properties of the free coumarin dyes; **L1** emits strongly while **L2** is only weakly emissive. On binding to Pt(acac) the strong fluorescence of **L1** is partially quenched while coumarin phosphorescence is observed from cyclometalated **L1** and **L2**. The ligand-centered nature of the LUMO was confirmed by IR spectroelectrochemistry while the assignment of the phosphorescence emission as ligand-based rests on the vibrational structuring, the negligible solvatochromism, the small temperature-induced Stokes shifts on cooling to 77 K, the emission lifetimes, and strong oxygen quenching. (TD-)DFT calculations confirm our experimental results and provide an assignment of the electronic transitions and the spin density distributions in the T_1 state.

1. Introduction

Platinum-based emitters with cyclometalating arylimine ligands derived from arylpyridines, arylthiazoles or -benzothiazoles or arylpyrazoles combine several attractive features such as an easy synthesis from well accessible precursors, good general stabilities, rather high quantum yields, and reasonably long lifetimes of their emission. Furthermore, their emission color is easily tuned by varying the substituents on the arene or imine constituents or the other coligand(s) [1–26]. The Pt coordination center with its high spin-orbit coupling constant serves to promote efficient intersystem crossing (ISC), hence populating a lower-lying excited triplet sate from excited singlet state(s), while, at the same time, promoting a relatively rapid decay of the T_1 state to the S_0 ground state by the same mechanism[19,23]. Cyclometalated Pt(II) complexes thus find applications as emitter materials for OLEDs, as sensitizers for electroluminescent devices or dye-based solar cells [5,7,15,16,22,27,28], as oxygen sensors [17,29,30], or for triplet-triplet-annihilation-based upconversion [9,30].

Particularly important are representatives where the other coligand is a β-diketonate, either acetylacetonate (acac) or its pivaloyl or bis(trifluoromethyl) (hfac) analogues, the latter providing better solubilities and diminished π-stacking. The success of those derivatives arises from the rigid, planar structure imposed by the two chelate ligands with bond angles rather close to the ideal values, their low propensity to tetrahedral distortion or twisting of one chelate plane with respect to the other in the excited state (the so-called D_{2d} distortion), and the strong ligand field imposed by the C^N cyclometalating ligand. All these factors prevent rapid radiationless decay from the emissive triplet state through thermal equilibration with higher-lying non-emissive d-states by introducing large ligand-field splitting [19,20].

A major drawback of such complexes is, however, their usually rather low absorption in the visible (Vis) with extinction coefficients rarely approaching 10^4. A possible way to circumvent that problem is to resort to a donor-acceptor-type architecture of the cyclometalating ligand which, by adding a strong intraligand charge-transfer component, red-shifts and intensifies the lowest-energy band [1,5,15,16,27,29] or the covalent attachment of a dye to the ligand. If the dye-based $^1\pi{\rightarrow}\pi^*$ state is energetically above the emissive triplet state it may well act as an antenna. Hence, the emissive triplet state, which mostly assumes a metal-to-ligand charge transfer (MLCT) character, is also populated by energy transfer from the excited $^1\pi{\rightarrow}\pi^*$ state of the dye [31,32]. Alternatively, the Pt atom can promote the otherwise forbidden ISC of the attached dye and thus populate an emissive ligand-based triplet state (^{3}IL), which then emits with much lower luminescence lifetimes when compared to the ^{3}IL ($^3\pi^*$) state of the parent dye [1,9,17,30,33–36]. To these ends, coumarins, and, in particular the benzothiazole-functionalized coumarin 6, have been repeatedly used as cyclometalating ligands and have been found to endow their metal complexes with interesting photophysical properties [1,30,32–35,37].

We here report on two Pt(acac) complexes with pyridyl-functionalized cyclometalating coumarins that differ with respect to the position of the pyridine-coumarin linkage. In these two complexes, the Pt atom is either attached to the lactonyl or the phenyl ring of the coumarin entity. We demonstrate that

the point of attachment and the substitution pattern influence the absorption and emission properties and either result in a relatively long-lived [3]IL or dual ligand-based fluorescence and phosphorescence emission. The electronic transitions and the nature of the emissive states are probed by quantum chemical calculations paired with IR spectroelectrochemical measurements.

2. Results and Discussion

2.1. Synthesis, NMR Spectroscopy, and Structural Characterization

Complexes **1** and **2** of this study are shown in Chart 1. Ligand **L1** is literature-known [38], while ligand **L2** was prepared by Negishi coupling from 4-methylcoumarin-7-trifluoromethanesulfonate (**4-MCOTf**) [39] and 2-pyridyl zinc chloride according to the method of Manabe [40] using diisopropyl(2-naphthyl)phosphine/Pd(OAc)$_2$ as the (pre)catalyst (Scheme 1) [41]. The synthesis of the cyclometalated platinum complexes **1** and **2** follows the well-established sequence of first reacting the corresponding arylpyridine with K$_2$[PtCl$_4$] or PtCl$_2$(dmso)$_2$ in water/2-methoxyethanol and then treating the resulting chloro-bridged dimers {(**L1**)PtCl}$_2$ or {(**L2**)PtCl}$_2$ with acetylacetone in the presence of Na$_2$CO$_3$ base in 2-methoxyethanol as the solvent (Scheme 2) [1,42,43]. Complexes **1** and **2** were obtained in overall yields of 17% and 63%, respectively, after purification by column chromatography (**1**) or recrystallization (**2**). The rather low yield of **1** is a consequence of its propensity to competing decomposition with release of **L1** under the reaction conditions and the tedious chromatographic purification.
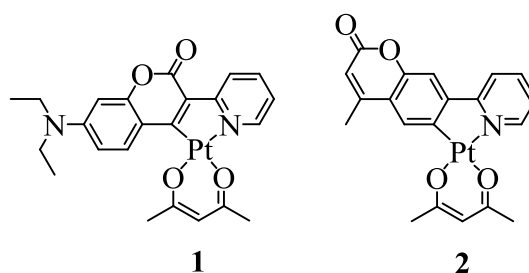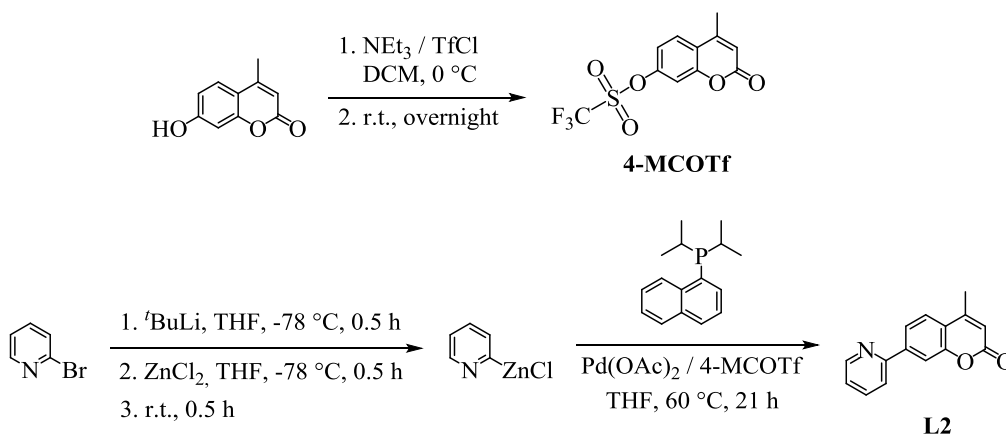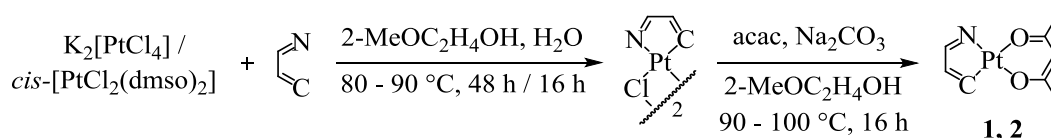

Chart 1. Structures of complexes **1** and **2**.

Scheme 1. Synthesis of ligand **L2**.

Scheme 2. Synthesis of complexes **1** and **2**.

Successful cyclometalation was evidenced by the loss of the resonance signal of the respective proton of the free ligand, appreciable downfield shifts of the resonance signal(s) of the proton(s) adjacent to the site of Pt attachment, and the additional splitting of these signals by $^3J_{Pt-H}$ satellites of *ca.* 15–20 Hz. We also note strong coordination shifts of 10.2, 11.9, and 6.3 ppm to lower field for the Pt-bonded carbon atom C6 and the quaternary carbon atoms that connect the two aromatic rings when comparing complex **2** and **L2** (see Experimental Section; NMR spectra are displayed as Figures S1-S7 of the Electronic Supporting Information (ESI)).

Single crystals for X-ray diffraction studies were obtained by layering saturated solutions of the complexes in dichloromethane (DCM) with petroleum ether. The molecular structures are displayed in Figure 1 along with the atomic numbering scheme, while Table 1 summarizes the most important bond lengths, bond angles, and dihedral angles. Details of the data collection, structure refinement, and full lists of metric parameters can be found as Tables S1–S3 of the ESI.
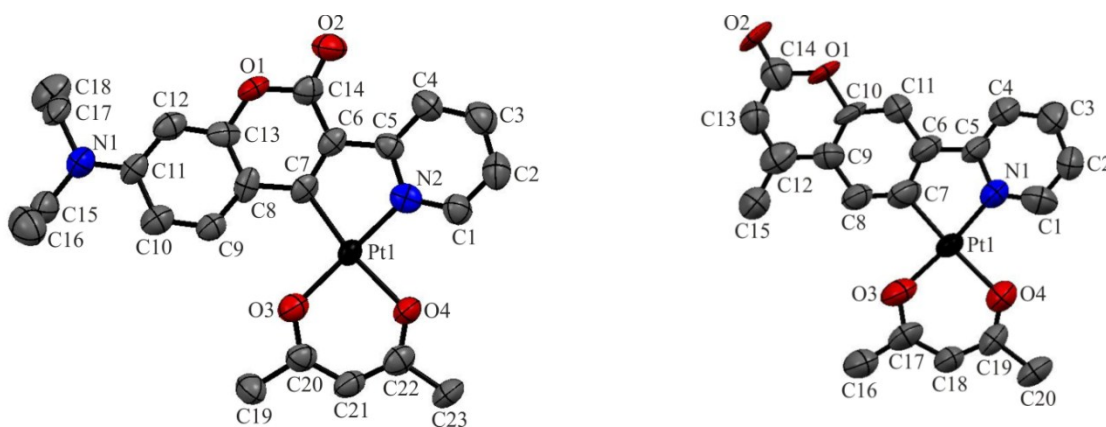

Figure 1. Structures of complexes **1** (**left**) and **2** (**right**). Hydrogen atoms are omitted for reasons of clarity; ellipsoids are drawn at a 90% probability level.

Angle sums of 359.9 (**1**) or 360.0° (**2**) at the coordination center indicate that the Pt(II) atom attains its typical square planar coordination geometry. Small distortions from the ideal geometry are imposed by the planar five-membered N^C chelate, which contracts the N-Pt-C bond angle to 81.3(2) (complex **1**) or 82.4(4)° (complex **2**) and concomitantly opens the other *cis*-angles. In complex **1**, only the adjacent angle C(7)-Pt-O(3) is affected and becomes obtuse at 99.0(2)°. In **2**, however, that effect is almost evenly distributed over all three remaining *cis*-angles, which are in the range of 91.2(4) to 93.5(3)°. Thus, in **1** the acac ligand bends over to the pyridyl ring of the cyclometalated C^N ligand while it is on-center in **2**. The small dihedral angles formed by the conjoint rings of the cyclometalated ligand or the aryl or pyridyl constituents of that chelate and the adjacent donor function of the acac ligand (Table 1) as well as the small interplanar angles between the normals to the best planes of the five-membered Pt(C^N) and the six-membered Pt(O^O) chelates of 5.70 (**1**) or 1.08° (**2**) attest to a high degree of

coplanarity with only a minute twist for complex **1**. This is an important prerequisite for good luminescence properties. At *ca.* 1.97 (N), 1.98 (C7), and 2.01 (O3) or 2.08 Å (O4) the Pt-N, Pt-C, and Pt-O bond lengths offer no peculiarities with respect to similar structures [1,3,5,6,29,44,45]. As usual, the Pt-O bond opposite the aryl C atom is considerably longer than that opposite the pyridine N donor as a consequence of the larger *trans* influence of the σ-bonded aryl ligand [44].

Table 1. Selected bond lengths [Å], bond angles [deg], and dihedral angles [deg] for complexes **1** and **2**.

Bond parameter	1	Bond parameter	2
Pt(1)-N(2)	1.974(5)	Pt(1)-N(1)	1.965(11)
Pt(1)-C(7)	1.978(6)	Pt(1)-C(7)	1.983(9)
Pt(1)-O(3)	2.013(4)	Pt(1)-O(3)	2.010(9)
Pt(1)-O(4)	2.072(4)	Pt(1)-O(4)	2.089(8)
O(1)-C(13)	1.379(7)	O(1)-C(13)	1.371(13)
O(1)-C(14)	1.382(7)	O(1)-C(14)	1.395(11)
O(2)-C(14)	1.221(7)	O(2)-C(14	1.241(14)
O(3)-C(20)	1.292(7)	O(3)-C(17)	1.284(13)
O(4)-C(22)	1.279(7)	O(4)-C(19)	1.283(14)
C(7)-Pt(1)-N(2)	81.3(2)	C(7)-Pt(1)-N(1)	82.4(4)
C(7)-Pt(1)-O(3)	99.0(2)	C(7)-Pt(1)-O(3)	91.2(4)
N(2)-Pt(1)-O(4)	89.64(18)	N(1)-Pt(1)-O(4)	93.5(3)
O(3)-Pt(1)-O(4)	89.91(16)	O(3)-Pt(1)-O(4)	92.9(3)
N(2)-Pt(1)-O(3)	176.67(16)	N(1)-Pt(1)-O(3)	173.6(3)
C(7)-Pt(1)-O(4)	170.40(18)	C(7)-Pt(1)-O(4)	175.9(4)
O(2)-C(14)-O(1)	114.7(5)	O(2)-C(14)-O(1)	116.3(10)
N(2)-C(5)-C(6)-C(7)	0.3(7)	N(1)-C(5)-C(6)-C(7)	-0.6(14)
N(2)-Pt(1)-O(4)-C(22)	-178.3(4)	N(1)-Pt(1)-O(4)-C(19)	178.0(9)
C(7)-Pt(1)-O(3)-C(20)	176.8(4)	C(7)-Pt(1)-O(3)-C(17)	-179.3(10)
O(3)-Pt(1)-C(7)-C(8)	4.9(5)	O(3)-Pt(1)-C(7)-C(8)	1.0(12)
O(4)-Pt(1)-N(2)-C(5)	173.0(4)	O(4)-Pt(1)-N(1)-C(5)	179.2(8)

In the crystal, complexes **1** and **2** show a variety of intermolecular interactions that lead to interesting packing motifs. Individual molecules of **1** arrange into staggered head-to-tail dimers that are held together by a short Pt···Pt contact and by π-stacking interactions between the electron-rich acac and the electron-poor pyridyl and coumarin lactonyl rings. Figure 2 provides two different views of these "dimers." The Pt···Pt distance of 3.164(1) Å is on the short end of such contacts [5,46,47] and well within a range that is usually only observed for dinuclear complexes, where such close contacts are enforced by small bridging ligands such as dppm [48–51] or in linear chain structures [52,53]. The planes of the Pt(O^O) and the Pt(C^N) chelate rings of the two associated molecules are only slightly tilted by 5.6° with a stacking distance of 3.33 Å as defined by the distance between the centroids of the Pt(acac) and the Pt,N(2),C(5),C(6),C(7) planes.
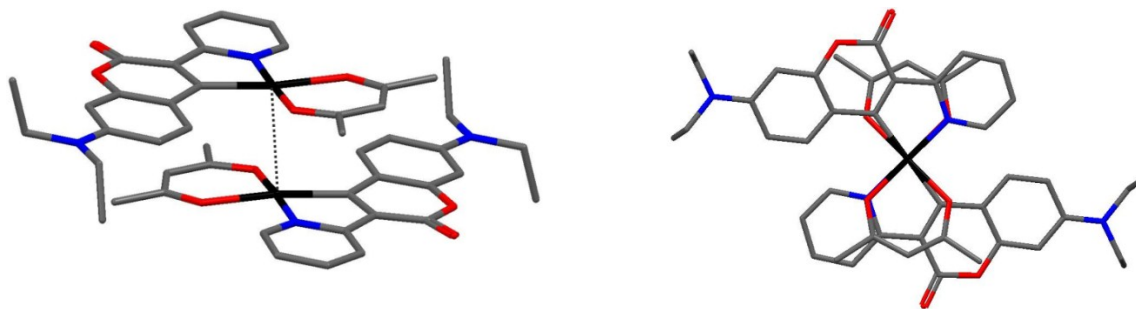
Figure 2. Side and top view on two molecules of **1** that associate through a short Pt···Pt contact of 3.164(1) Å and π-stacking of 3.33 Å.

Individual dimers in the crystal structure of complex **1** are laterally offset with respect to neighboring ones, which keeps the interdimer Pt atoms at a non-interacting distance of 4.988(1) Å. They nevertheless arrange in an exactly coplanar fashion as indicated by the angle of 0.0° between the planes defined by the coordination center and all atoms of the O^O and C^N chelates at an even closer stacking distance of 3.19 Å. This results in an association of individual dimers into one-dimensional stacks that run along the *a* axis of the unit cell. The close interdimer stacking places one methyl hydrogen atom of each acac ligand in proximity to the carbonyl O atom of the coumarin substituent to form pairwise contacts of 2.646 Å, which are 7 pm smaller than the sum of the van der Waals radii. This may additionally enforce the overall stacking of individual dimers. Molecules belonging to different stacks interact weakly by pairwise H···O hydrogen bonds of 2.660 Å along the *c* axis or of 2.690 Å along the *b* axis of the unit cell. These contacts form between one methyl hydrogen atom of the NMe2-substituent and the coumarin oxygen atom. The resulting pattern of hydrogen bonds is displayed in Figure S8 of the ESI while Figure S9 offers two different views of the stacking arrangement.

Individual molecules of complex **2** arrange into a 2D sheet structure, which mainly results from overlap between different constituents of coplanar arranged π-ligands. Each molecule interacts with two partners of the above sheet in a pairwise fashion via π-stacking interactions of 3.38 Å between the lactonyl part of the cyclometalating ligand and the pyridyl ring. Contacts to molecules of the sheet below are formed by pairwise π-stacking of the acac ligand of one molecule with the pyridyl ring of the other and *vice versa*, again with a stacking distance of 3.38 Å. These interactions are displayed in Figures 3 and S10 of the ESI. Further contacts to yet another molecule of the sheet below are formed by pairwise hydrogen bonding interactions that involve one methyl hydrogen atom and one oxygen atom of the acac ligand. These interactions of 2.702 Å are, however, only 2 pm shorter than the sum of the van der Waals radii. Additional interactions within each individual sheet involve rather close contacts of 2.454 Å or 2.570 Å between the exocyclic coumarin carbonyl oxygen atom and hydrogen atom H(4) of the pyridyl or methyl hydrogen atom H(15) of the acac ligand, respectively, of two different neighbor molecules. These contacts are 27 or 15 pm shorter than the sum of the van der Waals radii and are displayed in Figure S11 of the ESI.
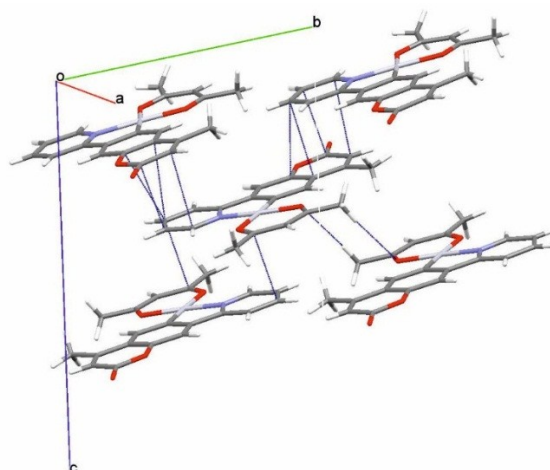
Figure 3. Packing of individual molecules of complex **2** in the crystal, displaying the different interactions of the molecule in the middle with four partners belonging to the sheets above and below. Close contacts are indicated by dark blue dotted lines.

2.2. Absorption and Emission Properties

Ligands **L1** and **L2** differ strongly with respect to their optical properties. In CH_2Cl_2 **L2** shows a broad, structured absorption with individual peak maxima at 306 and 330 nm and an additional shoulder near 350 nm; extinction coefficients are of the order of *ca.* 1.6×10^4 M^{-1} cm^{-1} (see Figure 4 and Table 2). In contrast, **L1** has a red-shifted and appreciably more intense absorption at λ_{max} = 414 nm ($\varepsilon = 3.5 \times 10^4$ M^{-1} cm^{-1}), suggesting that the underlying transition comprises some charge-transfer components from the NMe_2 donor to the electron-accepting lactonyl and pyridyl constituents of **L1** [38]. Similar findings have also been reported for dialkyl- or diarylamino-substituted coumarins [5,29,30,33−35,54]. Clear differences are also seen in the emission spectra: While **L1** emits intensely at 470 nm with a quantum yield of 83%, **L2** is only weakly emissive ($\Phi_F = 3.6\%$) at r. t. in solution (Table 3).
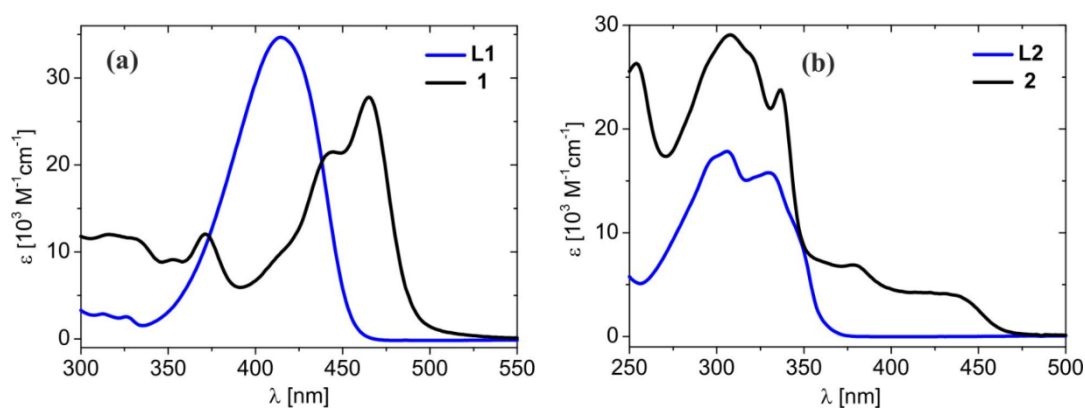

Figure 4. Comparison of the electronic absorption spectra of (**a**) **L1** and **1**; (**b**) **L2** and **2** in CH_2Cl_2 solution.

The differences in the absorption spectra of **L1** and **L2** also prevail in their complexes **1** and **2**. Thus, the π→π* absorptions of the parent coumarin dye are fully preserved in complex **2** and their positions are only very slightly shifted with respect to the free dye. Additional, weaker bands appear at

lower energies, suggesting some contribution of the Pt(acac) moiety to these transitions. The latter notion is further substantiated by the moderate yet observable negative solvatochromism of these bands [55], which also indicates that the underlying excitations involve some limited degree of charge transfer (Table 2).

Table 2. Electronic absorption data for complexes **1** and **2** in different solvents.

Compound	Solvent	λ_{max} [nm], (ε_{max} [10^4 M^{-1}cm^{-1}])
L1	DCM	273 (1.05), 414 (3.50)
L2	DCM	223 (2.05), 306 (1.78), 330 (1.58)
	MeCN	265 (2.16), 317 (1.25), 369 (1.40), 462 (3.32)
1	DCM	268 (1.93), 316 (1.18), 371 (1.19), 465 (2.76)
	THF	262 (2.31), 320 (1.31), 371 (1.67), 464 (3.29)
	MeCN	251 (1.87), 304 (1.98), 333 (1.64), 377 (0.37), 416 (0.33), 426 (0.33)
2	DCM	254 (2.63), 308 (2.91), 337 (2.38), 379 (0.69), 422 (0.42), 432 (0.41)
	THF	252 (2.77), 308 (2.83), 338 (2.26), 388 (0.50), 427 (0.44), 439 (0.43)

For complex **1**, the main absorption experiences a distinct red shift of 2650 cm^{-1} and now appears as a vibrationally structured band. In contrast to the **L2/2** couple of compounds, the absorptivity is somewhat reduced on metal coordination. A second distinct peak that has no equivalent in free **L1** is seen in the near UV at 371 nm. With a view to related complexes, that peak is assigned to an MLCT transition [1,3,54]. In agreement with that notion, the respective band is clearly solvatochromic (see Figure 5 and Table 2). Additional, weaker features show up deeper in the UV with increased intensities when compared to the free ligand **L1** (see Figures 4,5 and Table 2). All these bands are nearly invariant to the solvent, indicating only small changes in the polarities of the involved states (Figure 5).
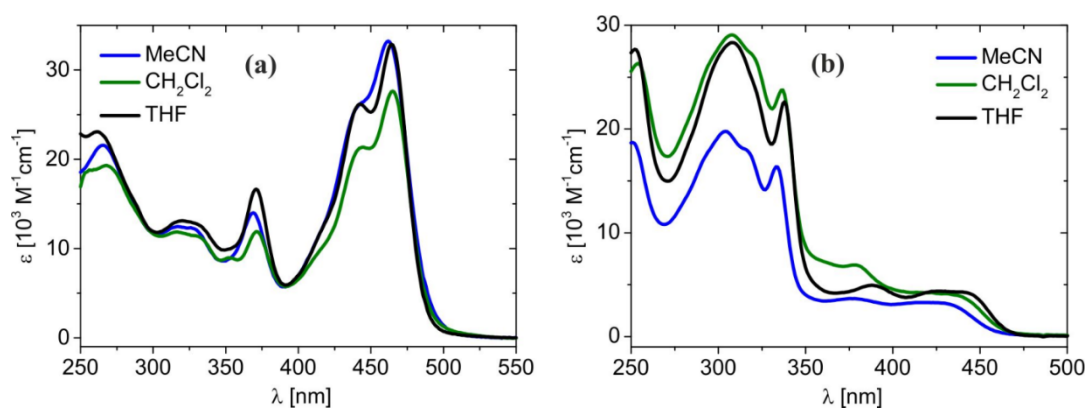

Figure 5. Electronic absorption spectra of complexes **1** (**a**) and **2** (**b**) in different solvents.

Insight into the nature of the relevant transitions and involved states was sought by (TD-)DFT calculations on the fully optimized structures of complexes **1** and **2**. We note that the PBE0-calculated structures reproduce the experimental parameters better than the B3LYP ones (see Tables S9 and S10 of the ESI), while the latter functional gives a better match between calculated and experimental spectra (see Figure S18 of the ESI). The B3LYP-calculated spectra reproduce the general absorption features very well but overestimate transition energies by about 1700 cm^{-1}, which is not uncommon for such complexes. Only one strong visible absorption feature at 431 nm is calculated for complex **1**,

which further argues for a vibrational origin of the experimentally observed band structuring. That main absorption originates from the HOMO→LUMO transition and is best described as a π→π* transition within the cyclometalated coumarin dye with some degree of charge-transfer (CT) from the electron-rich dimethylaminophenyl ring to the electron accepting lactonyl and pyridyl constituents of the cyclometalating ligand. The additional, weaker excitations in the (near) UV at calculated wavelengths of 345 and 324 nm are mainly HOMO-1→LUMO and HOMO→LUMO+2 in character. They involve transitions from a state with strong Pt(acac) contributions of 72% to the same acceptor orbital (λ_{calc} = 345 nm) and a π→π* transition with a minor coumarin→acac (L→L') component (λ_{calc} = 324 nm). These transitions most likely account for the bands at 370 nm and the lower energy part of the composite band near 320 nm. They are followed by a set of two likewise closely spaced transitions mainly of a HOMO-2→LUMO+1 (λ_{calc} = 287 nm) and HOMO-1→LUMO+3 (λ_{calc} = 244 nm) character. Graphical representations of the relevant molecular orbitals are provided in Figure 6. A full list of calculated electronic transitions, fragment contributions to the relevant MOs in the frontier orbital (FMO) region and a more complete set of graphical MO representations can be found as Tables S6 and S8 and Figure S19 of the ESI.
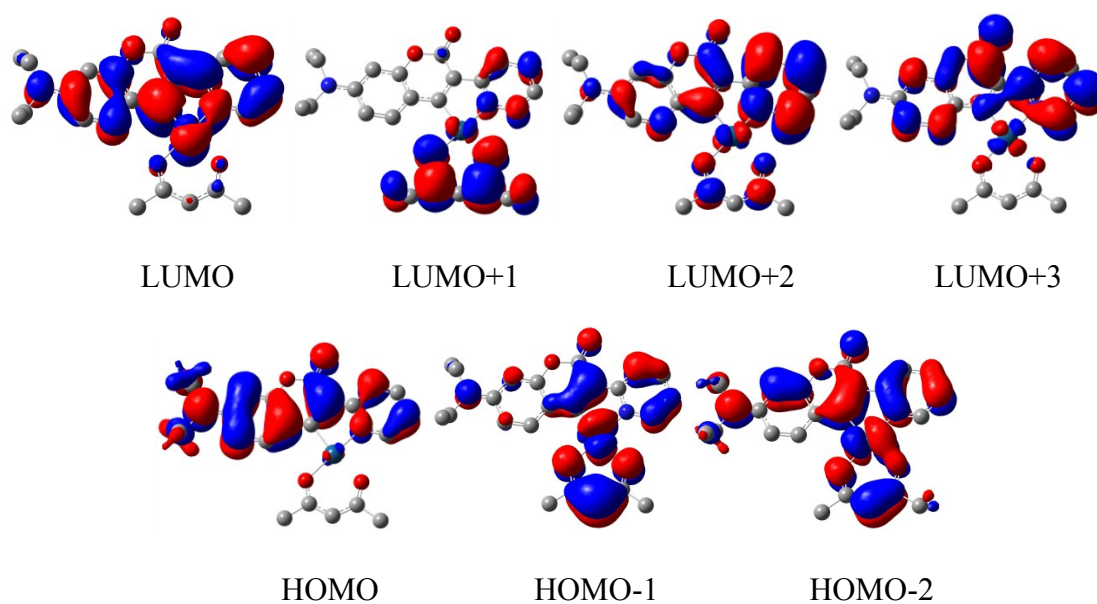

LUMO   LUMO+1   LUMO+2   LUMO+3

HOMO   HOMO-1   HOMO-2

Figure 6. Selected molecular orbitals of complex **1** in the FMO region.

Selected FMOs of complex **2** that are relevant for the observed electronic transitions are displayed in Figure 7; listings of fragment contributions and TD-DFT calculated transitions and a more complete set of calculated MOs may be found as Tables S7 and S8 and Figure S20 of the ESI. In contrast to complex **1**, the donor orbitals HOMO and HOMO-1 are delocalized over the cyclometalating coumarin–pyridine hybrid ligand and the Pt(acac) moieties with a dominant contribution of the negatively charged coumarinyl part of **L2** to the HOMO. As for complex **1**, the LUMO is essentially delocalized over the dye ligand with rather similar contributions from the coumarin and pyridyl subunits. The absence of a strong donor substituent and the shift of the site of pyridyl attachment from the lactonyl to the phenyl part of the coumarin thus have the combined effect of decreasing the polarization of the MOs having strong contributions of the cyclometalating ligand when compared to complex **1**.
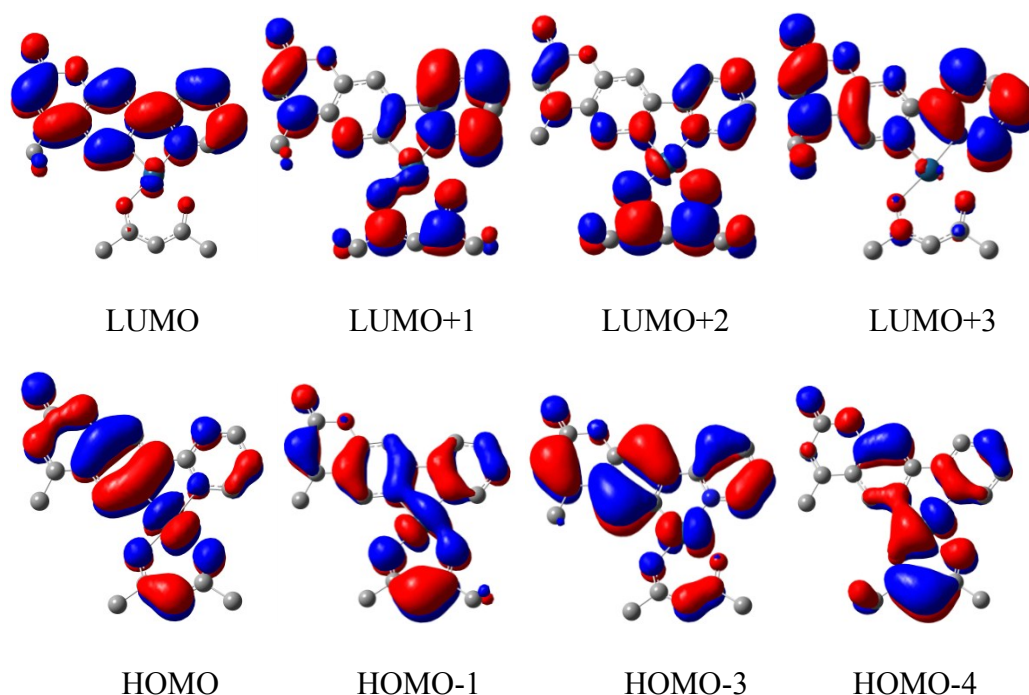
| LUMO | LUMO+1 | LUMO+2 | LUMO+3 |

| HOMO | HOMO-1 | HOMO-3 | HOMO-4 |

Figure 7. Selected molecular orbitals of complex **2** in the FMO region.

The calculated HOMO→LUMO transition underlying the band at λ_{calc} = 422 nm is thus best described as a blend of intraligand CT from the phenyl part of the cyclometalated ligand to the appended pyridyl and lactonyl acceptor units and CT from the Pt(acac) moiety to the cyclometalating ligand. That transition most likely accounts for the lowest energy band of complex **2** at 432 nm. It is followed by a second band of likewise moderate absorptivity, which is assigned as the excitation from HOMO-1 to the same acceptor orbital with some larger degree of CT from the Pt(acac) fragment. The most intense band of the electronic spectrum at λ_{calc} = 320 nm arises mainly from the HOMO-3→LUMO excitation. Like for complex **1**, it is essentially a π→π* type transition within the cyclometalated ligand, with some minor degree of electron donation from the Pt(acac) fragment. This transition most likely accounts for the low-energy part of the strong, broad feature in the experimental absorption spectrum. Other components of that composite band have a strongly mixed character, with involvement of several different MOs down to HOMO-9 and up to LUMO+5 (see Table S7 of the ESI).

Electrochemistry is a potent tool to probe for the energies of the immediate frontier MOs. In cyclic voltammetry (DCM, 0.1 M NBu$_4$PF$_6$, r. t.), complex **1** displays an irreversible oxidation at a peak potential E_p of 0.53 V. On extending the anodic scan to more positive values a second, likewise chemically irreversible process is observed at E_p = 0.67 V. The associated peak current is considerably smaller than that of the initial process and does not vary appreciably with sweep rate, which does not allow us to assign it to either the second oxidation of **1** or to a product generated during the decomposition of its oxidized form. The cathodic scan (THF, 0.1 M NBu$_4$PF$_6$, r. t.) reveals a chemically reversible ($i_{p,a}/i_{p,c}$ = 1.0; $i_{p,a}$ and $i_{p,c}$ denote the anodic and cathodic peak currents of the wave) reduction at a half-wave potential $E_{1/2}$ of -2.27 V. Representative voltammograms of complex **1** are displayed as Figure S15 of the ESI.

As complex **2** lacks the NMe$_2$ donor substituent of complex **1** its FMO energies are expected to be lower. Indeed, calculated energies are −5.76 eV for the HOMO and −2.24 eV for the LUMO as

compared to −5.22 eV and −1.93 eV for complex **1**. As a consequence the oxidation and reduction potentials are shifted anodically with respect to **1**. Thus, the peak of the irreversible oxidation appears at 0.65 V (here one should, however, bear in mind that the peak potentials of chemically irreversible electrode processes provide no stringent thermodynamic information but are also influenced by the rate and equilibrium constant of the chemical follow-up process). Notwithstanding, the $E_{1/2}$ of the first, chemically reversible reduction of complex **2** is −2.09 V and hence by 180 mV more positive than that of complex **1**. In further contrast to **1**, complex **2** can be reduced by one further electron within the potential window of the THF/0.1 M NBu$_4$PF$_6$ supporting electrolyte. The second reduction gives rise to a chemically partially reversible process ($i_{p,a}/i_{p,c} \approx 0.7$) at $E_{1/2} = -2.40$ V (see Figure S16 of the ESI).

This provided us with the opportunity to directly probe for the identity of the primary reduction site by means of IR spectroelectrochemistry. Considering that the LUMO of complex **2** is entirely based on the coumarin/pyridyl-derived ligand **L2**, reduction should induce major changes of the ligand-based stretches and, in particular, those associated with the lactonyl moiety.

In their IR spectrum the free ligand **L2** and complex **2** both feature a weak band near 1770 cm^{-1} and a prominent absorption at 1715 cm^{-1} that can be assigned to the lactonyl moiety of the coumarin (see Figures S12 and S14 of the ESI). Additional rather intense bands of complex **2** are observed in the region above 1500 cm^{-1} with prominent peaks at 1576, 1563, and 1514 cm^{-1} in the solid or at 1577, 1564, and 1522 cm^{-1} in THF solution. IR spectroscopic changes on reduction were monitored under *in situ* conditions in an optically transparent thin-layer electrolysis (OTTLE) cell based on the design of Hartl *et al.* [56]. On stepwise reduction to first the radical anion **2**$^{-}$ and then to dianion **2**$^{2-}$ the original carbonyl bands bleach out while intense bands at 1673 and 1644 cm^{-1} (**2**$^{-}$) and then at 1604 cm^{-1} (**2**$^{2-}$) appear (Figure 8), thus indicating a stepwise shift of the lactonyl band to lower energies on negative charging. Both reductions are notably accompanied by distinct sets of isosbestic points, attesting to clean conversions, even for the second reduction step. These observations support our notion that the LUMO of **2** is centered on the cyclometalating ligand.

Table 3 summarizes the photophysical data for the free ligands **L1**, **L2** and their associated Pt(acac) complexes **1** and **2**. While uncoordinated **L2** is only weakly emissive ($\Phi_F = 3.6\%$), complex **2**, on excitation into the low-energy absorption band, shows a rather intense, vibrationally structured emission with a quantum yield Φ of 21.3%. Very similar results were obtained in 2-MeTHF with only small differences with respect to emission wavelength and quantum yield. The main peak at 550 nm is the most blue-shifted one; additional, less intense peaks are found at 594 and 640 nm (see Figure 9). The large Stokes shift of 4970 cm^{-1} and the strong quenching by atmospheric oxygen indicate phosphorescence emission from the T$_1$ state. Vibrational structuring is a characteristic asset of a ^{3}IL-based emission arising from a ligand-centered excited state where the heavy metal atom has only small contributions but efficiently triggers the otherwise forbidden S$_1 \rightarrow$ T$_1$ intersystem crossing (ISC) of a coordinated ligand owing to its large spin-orbit coupling constant [19]. Typical examples of such behavior are Pt alkynyl complexes [57–67]. The latter notion is further supported by the computed spin density surface for the T$_1$ state of complex **2** as it is depicted in Figure 10a. Thus, the unpaired spins are evenly distributed over the cyclometalated coumarin–pyridyl ligand, with only small contributions from the Pt atom.
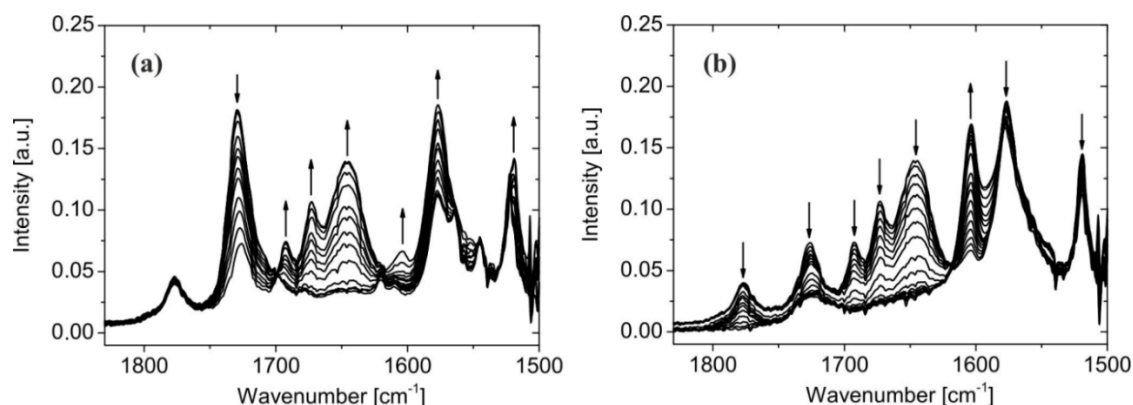
Figure 8. Spectroscopic changes in the IR during electrochemical reduction of complex **2** to **2⁻** (**a**) and of **2⁻** to **2²⁻** (**b**) in a 0.2 M NBu₄PF₆/THF solution at r. t.
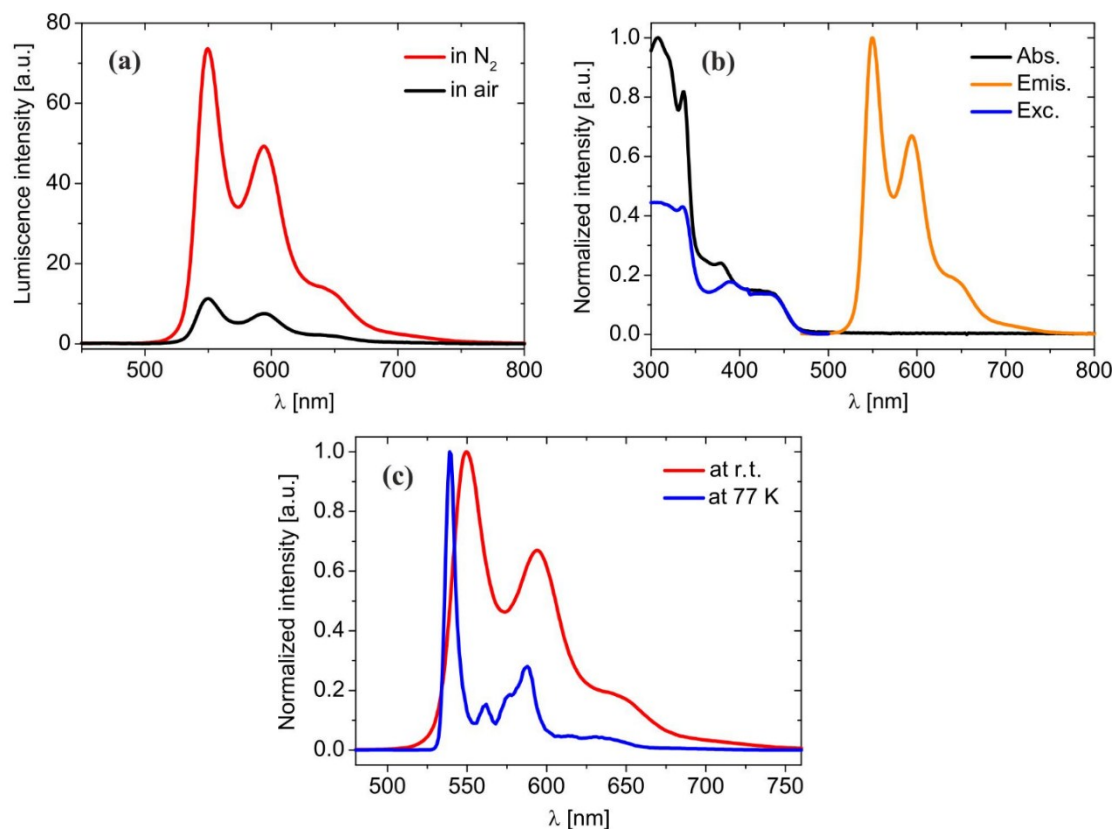

Figure 9. Emission spectra of aerated and deoxygenated solutions of **2** (**a**) in DCM recorded at λ_{exc} = 412 nm; (**b**) comparison of the absorption, emission, and excitation spectra (λ = 550 nm) of **2** in DCM at r. t.; (**c**) comparison of emission spectra of **2** at r. t. and at T = 77 K in a frozen 2-MeTHF matrix.

At r. t. the lifetime of the emission is 1.6 µs. While such a lifetime would be extremely short for a purely organic phosphor, it is rather typical of the triplet emission of a complex, where higher lying and thermally accessible states with high metal contribution provide a pathway for radiationless decay [19]. In keeping with that hypothesis, the emission lifetime increases to 15.3 µs in a frozen 2-MeTHF matrix. Under these conditions further sharpening and resolution of vibrational sublevels is

observed along with only a slight solvent- and matrix-induced blue shift of the main peak to 539 nm (Figure 9c). We note here that weak solvatochromism and small thermally induced Stokes shifts are well-established tokens of ligand-based emissions [8,33,68].

Excitation spectra recorded at $\lambda = 550$ nm retrace the features of the absorption spectrum, yet with reduced intensities of the multiple UV transitions (see Figure 9(b)). This probably indicates that only some components of the highly mixed transitions in the UV (*vide supra*) populate the lower-lying emissive ligand-centered T_1 state.

Table 3. Photophysical data for ligands **L1** and **L2** and complexes 1 and 2 in DCM (r. t.) or 2-MeTHF ($T = 77$ K).

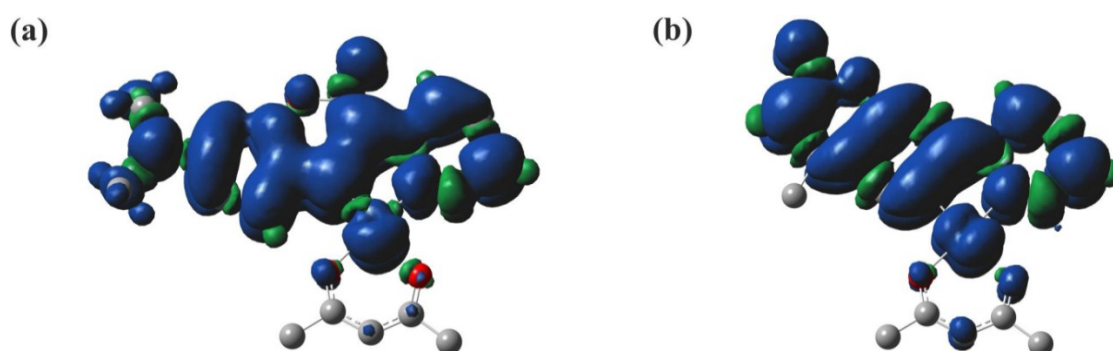| Compound	λ_{max} [nm], (ε_{max} [10^4 M^{-1}cm^{-1}])	$\lambda_{em\ r.t.\ /\ 77\ K}$ [nm]	$\Phi_{F/P}$	$\tau_{r.t./77\ K}$ [μs]
L1	414 (3.50)	470 F	0.83 [38]	0.0026
L2	223 (2.05), 306 (1.78), 330 (1.58)	376 F	0.036	-
1	268 (1.95), 316 (1.20), 371 (1.21), 465 (2.78)	457 F, 486 F, 566/454 F, 486 F,	0.064/0.210	0.0026 F 12.4/103.3
2	254 (2.63), 308 (2.91), 337 (2.38), 379 (0.69), 422 (0.42) 432 (0.41)	550/539	-/0.213	1.6/15.3

F denotes fluorescence.

Figure 10. Spin-density surfaces for the triplet states T_1 of complexes **1 (a)** and **2 (b)**.

On excitation at $\lambda = 420$ nm, complex **1** displays a similarly structured emission, which, on account of the Stokes shift of 3840 cm^{-1} and the almost quantitative quenching under atmospheric oxygen, is likewise assigned as phosphorescence from the T_1 state. The quantum yield of 21.0% is essentially identical to that of complex **2** whereas the emission lifetime of 12.4 μs at r. t. is appreciably longer. Again, the behavior in 2-MeTHF was very similar. The calculated spin density map closely resembles that of complex **2** and reasserts that the phosphorescence emission is also ligand-based.

In striking contrast to complex **2**, however, complex **1** also fluoresces with a main peak at $\lambda = 486$ nm, a pronounced shoulder at 457 nm, and a quantum yield of 6.4% at r. t. The latter emission is invariant to atmospheric oxygen (see Figure 11) and its lifetime is 2.6 ns. In a rigid glassy 2-MeTHF matrix at $T = 77$ K all emission peaks are seen to sharpen. As a consequence the composite fluorescence emission is resolved into two separate peaks at essentially identical wavelengths as in a fluid solution. As for complex **2**, the fine structuring of the phosphorescence emission is enhanced along with a slight

blue-shift of the main emission peak to 557 nm (Table 3) while the lifetime of the phosphorescence emission increases to a remarkable value of 103 µs.
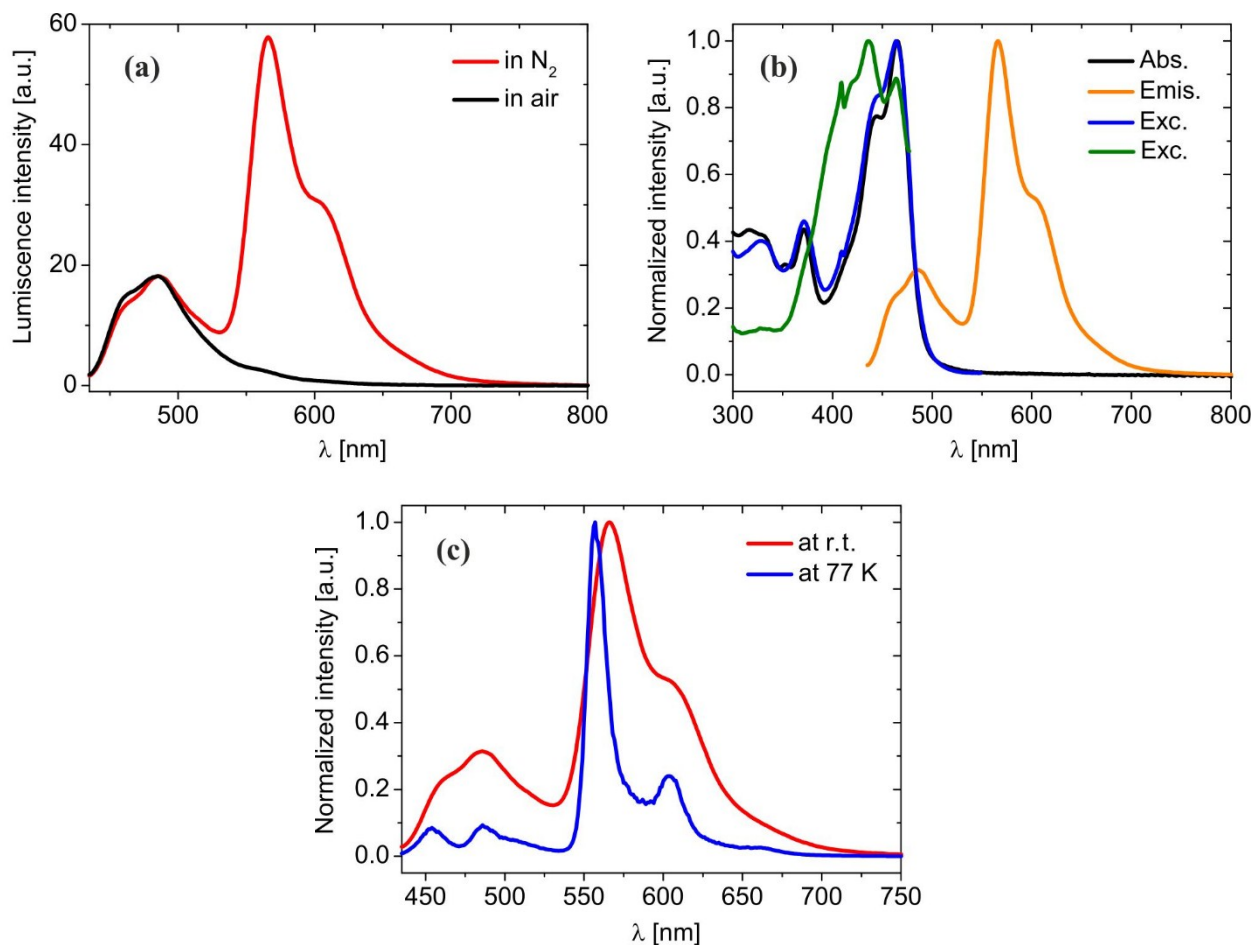

Figure 11. Emission spectra of aerated and deoxygenated samples of complex **1** (**a**) in DCM solution λ_{exc} = 420 nm; (**b**) comparison of the absorption, emission, and excitation spectra at λ = 565 nm (blue) and λ = 477 nm (green) in DCM at r. t.; (**c**) emission spectra at r. t. in DCM and at T = 77 K (λ_{exc} = 400 nm) in frozen 2-MeTHF.

Excitation spectra recorded at the peak of the phosphorescence and well within the envelope of the fluorescence emission retrace important features of the absorption spectrum. Given the high fluorescence quantum yield of **L1** of 83% and the fact that the high energy portion of the fluorescence excitation spectrum closely resembles features in the absorption spectrum of **L1**, it is likely that the fluorescence peak at the higher energy originates from trace impurities of free **L1** that are neither observed in NMR spectra nor show up in the absorption spectrum of **1**. In that respect we note that small quantities of free **L1** may be released during the observed slow decomposition of complex **1** in solution, particularly under UV irradiation. It should be emphasized, though, that the fluorescence excitation spectrum also features a prominent peak at 465 nm, which is specific to **1** and completely absent in **L1**. We thus conclude that complex **1** indeed shows dual ligand-based fluorescence and phosphorescence emission. Whilst not unprecedented, dual emission from the S$_1$ and the T$_1$ states from a metal-bonded ligand in a platinum or palladium complex is still rare and has been observed on only a few occasions [36,54,69–71]. Key to the observation of dual emission is that the Pt coordination center

has only limited contribution to the relevant frontier orbitals, as is the case here (see Figures 6 and 10). Another prerequisite is that the ISC rate resembles that of the fluorescence emission. We note that complexes exhibiting dual fluorescence and phosphorescence emissions have already been used as luminescence sensors for the quantitative detection of singlet-oxygen [70]. Such dual emitters have some advantages over two-component sensor systems in that there is no need to account for different bleaching rates of the phosphorescent sensor and the fluorescent standard that is needed for quantifying phosphorescence quenching by oxygen.

To conclude, binding of the pyridyl-functionalized coumarins **L1** and **L2** as cyclometalating ligands to the Pt(acac) fragment has the effect of turning on room temperature phosphorescence emission with a quantum yield of *ca*. 21% and partial quenching of the strong fluorescence emission of **L1**. Thus, while the site of pyridyl attachment to the coumarin dye and the presence of the NMe_2 donor have profound impact on the absorption and emission properties of the free ligands (**L1** absorbing strongly in the visible and being a very strong emitter whereas **L2** absorbs exclusively in the UV and is only weakly emissive), both ligands perform equally well in terms of quantum efficiency when cyclometalated to Pt(acac) with similar emission wavelengths of 566 and 550 nm, respectively. Experimental and quantum chemical studies show that both complexes emit from a metal-perturbed ligand-centered triplet state. Hence, the role of the heavy metal ion is to trigger the intersystem crossing of the ligand and to render the triplet state emissive with a comparatively short phosphorescence lifetime. Complex **1**, featuring that ligand, is a further example of the still rare class of complexes showing dual fluorescence and phosphorescence emissions.

3. Experimental Section

3.1. Materials and General Methods

All reactions were performed under an atmosphere of nitrogen using standard Schlenk techniques. THF and MeOH were dried by standard procedures. All solvents used for reactions or analytical purposes were degassed by saturation with nitrogen or by three freeze-pump-thaw cycles prior to use. All reagents were commercially available and used without further purification. Ligand **L1** [38], 4-methylcoumarin-7-trifluoromethanesulfonate (4-MCOTf) [39], and $PtCl_2(dmso)_2$ [72] were prepared according to literature procedures.

Infrared spectra were measured on a Perkin Elmer Spectrum 100 Series ATR-FT-IR spectrometer. NMR spectra were recorded on a Bruker Avance III 400 Automation or a Bruker Avance III 600 Cryoplatform as $CDCl_3$ or as CD_2Cl_2 solutions at 298 K. ^1H NMR spectra were referenced to the signal of the residual protonated solvent, ^{13}C NMR spectra to the solvent signal, and ^{31}P NMR spectra to an external standard (85% H_3PO_4). The assignment of ^1H and ^{13}C signals was supported by $^1H,^1H$-COSY, $^1H,^1H$-TOCSY, $^1H,^{13}C$-gHSQC, and $^1H,^{13}C$-gHMBC measurements. Elemental analyses (C, H, N) were performed at in-house facilities. Mass spectra were measured on a FAB-MS modified Finnigan MAT 312 spectrometer.

X-Ray diffraction analysis was performed on a STOE IPDS-II diffractometer equipped with a graphite-monochromated radiation source ($\lambda = 0.71073$ Å) and an image plate detection system at 100 K. The structures were solved by direct methods (SHELXS-97), completed with difference Fourier

syntheses, and refined with full-matrix least-squares using SHELXL-97 [73] minimizing $\omega(F_0{}^2 - F_c{}^2)^2$. Molecular structures in this work are plotted with Mercury 3.1.

UV-Vis electronic absorption spectra in acetonitrile, dichloromethane (DCM), and THF were obtained at ambient conditions in HELLMA quartz cuvettes with 0.1 cm optical path lengths on a TIDAS Diode-Array PGS NIR und MCS UV/NIR spectrometer from j&m Analytik AG. Emission and excitation spectra in degassed dichloromethane (DCM) at room temperature were recorded on a Perkin Elmer Luminescence spectrometer LS 50 in quartz cuvettes from HELLMA that were modified by glass joints, allowing spectra to be recorded under rigorous exclusion of air. The absorbance of all samples amounted to 0.04 to 0.06. Steady-state luminescence spectra at 77 K were recorded on a Fluorolog-3 instrument (FL322) from Horiba Jobin Yvon. Time-resolved luminescence spectra were measured on a LP920-KS instrument from Edinburgh Instruments equipped with an R928 photomultiplier and an iCCD camera from Andor. Luminescence was excited with the frequency-doubled output from a Quantel Brilliant b laser and the pulse length of approximately 10 ns or at a luminescence spectrometer picoQuant FT-300 with time-resolved single photon counting. Modified quartz cuvettes and tubes were employed for these optical spectroscopic experiments. The concentration of samples was *ca.* 1.5×10^{-5} M. Electrochemical investigations in degassed THF were performed in a vacuum tight one-compartment cell on a BAS CV50 potentiostat using Pt or glassy carbon disk electrodes from BAS as the working electrode, a Pt counter electrode, and a Ag pseudoreference electrode. Potentials were measured by adding decamethylferrocene (Cp^*_2Fe) and were referenced to the ferrocene/ferrocenium couple (under our conditions the half-wave potential of the $Cp^*_2Fe^{0/+}$ couple is −550 mV in CH_2Cl_2 or −455 mV in THF with respect to the $Cp_2Fe^{0/+}$). The design of the spectroelectrochemical cell follows that of Hartl *et al.* [56].

3.2. Quantum Chemical Calculations

The ground state electronic structures were calculated by density functional theory (DFT) methods using the Gaussian 09 [74] program packages. Quantum chemical studies were performed without any symmetry constraints. Open shell systems were calculated by the unrestricted Kohn–Sham approach (UKS) [75]. Geometry optimization followed by vibrational analysis was made either in vacuum or in solvent media. The quasirelativistic Wood–Boring small-core pseudopotentials (MWB) [76,77] and the corresponding optimized set of basis functions [78] for Pt and 6-31G(d) polarized double-ζ basis sets [79] for the remaining atoms were employed together with the Perdew, Burke, Ernzerhof (PBE0) [80,81], or the Becke exchange and correlation functional (B3LYP) [82,83]. Solvent effects were described by the polarizable conductor continuum model (PCM) [84–87] with standard parameters for dichloroethane. Absorption spectra and orbital energies were calculated using time-dependent DFT (TD-DFT) [88] and the same functional/basis set combinations mentioned above. For easier comparison with the experiment, the obtained absorptions were converted into wavelengths and broadened by a Gaussian distribution (full width at half maximum = 3000 cm^{-1}) using the program GaussSum [89]. Molecular orbitals were visualized with the GaussView program [90].
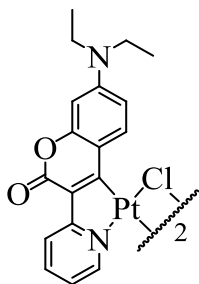
Bis-{μ-chloro-[7-diethylamino-3-(pyridin-2-yl)-*2H*-chromen-2-onato-*N'*,*C⁴*)]platinum(II)},

[(DAPC)Pt(μ-Cl)]₂: 7-Diethylamino-3-(pyridin-2-yl)coumarin (**L1**, 590 mg, 2 mmol) and K₂[PtCl₄] (830 mg, 2 mmol) were suspended in 32 mL of a water/2-methoxyethanol mixture (1:3). The reaction mixture was heated to reflux for 48 h at 80 °C. The obtained dark green solution was cooled to 0 °C and 70 mL of purified water were added. A brown precipitate was filtered off, washed with ethanol, and dried *in vacuo*. Yield: 650 mg, 0.72 mmol, 72%.
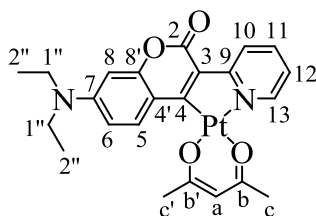
(7-Diethylamino-3-(pyridin-2-yl)-*2H*-chromen-2-onato-*N'*,*C⁴*)(2,4-pentanedionato-*O,O*)-platinum(II)
(1): [(DAPC)Pt(μ-Cl)]₂ (650 mg, 0.72 mmol), acetylacetone (0.22 mL, 2.16 mmol) and Na₂CO₃ (760 mg, 7.2 mmol) were suspended in 18 mL of 2-methoxyethanol and refluxed for 16 h at 100 °C. The precipitated crude product was filtered off and the residue was repeatedly extracted with 20 mL portions of dichloromethane. The combined organic phases were concentrated to a total volume of 20 mL. The product was purified by column chromatography on aluminum oxide (dichloromethane) to provide an orange solid. Yield: 150 mg, 0.25 mmol, 17%.

¹H-NMR (400 MHz, CDCl₃), δ = 8.95 (1H, d, *5-H*, $^3J_{HH}$ = 9.03 Hz), 8.85 (1H, d, *13-H*, $^3J_{HH}$ = 6.00 Hz, $^3J_{PtH}$ = 20.50 Hz), 8.51 (1H, d, *10-H*, $^3J_{HH}$ = 8.52 Hz), 7.71 (1H, pt, *11-H*, $^3J_{HH}$ = 8.52 Hz, $^3J_{HH'}$ = 7.42 Hz), 6.94 (1H, pt, *12-H*, $^3J_{HH}$ = 7.42 Hz, $^3J_{HH'}$ = 6.00 Hz), 6.54 (1H, dd, *6-H*, $^3J_{HH}$ = 9.03 Hz, $^4J_{HH}$ = 2.46 Hz), 6.40 (1H, d, *8-H*, $^4J_{HH}$ = 2.46 Hz), 5.45 (1H, s, *a-H*), 3.46 (4H, q, *1''-H*, $^3J_{HH}$ = 7.08 Hz), 1.95 (3H, s, *c'-H*), 1.94 (3H, s, *c-H*), 1.23 (3H, t, *2''-H*, $^3J_{HH}$ = 7.08 Hz), 1.20 (3H, t, *2'-H*, $^3J_{HH}$ = 7.08 Hz) ppm.

¹³C-NMR (100.6 MHz, CDCl₃), δ = 186.1 (s, *b-C*), 183.6 (s, *b'-C*), 167.7 (s, *9-C*), 167.0 (s, *4-C*), 157.6 (s, *2-C*), 155.4 (s, *8'-C*), 151.3 (s, *7-C*), 145.7 (s, *13-C*), 138.5 (s, *11-C*), 132.6 (s, *5-C*), 122.7 (s, *3-C*), 122.7 (s, *10-C*), 118.7 (s, *12-C*), 118.1 (s, *4'-C*), 108.3 (s, *6-C*), 102.6 (s, *a-C*), 96.3 (s, *8-C*), 44.8 (s, *1''-C*), 28.1 (s, *c-C*), 26.6 (s, *c'-C*), 12.9 (s, *2''-C*) ppm.

IR (cm⁻¹): ν(C=O) = 1763 vw, 1754 vw, 1711 w, 1678 vs, 1650 sh.

MS (FAB) *m/z* **(%)**: 589 (0.6) [M⁺ (¹⁹⁶Pt)], 588 (1) [M⁺ (¹⁹⁵Pt)], 587 (1) [M⁺ (¹⁹⁴Pt)].

Analysis calculated for C₂₃H₂₄N₂O₄Pt (587.53): C, 47.02%; H, 4.12%; N, 4.77%; found: C, 46.50%; H, 4.20%; N, 4.89%.
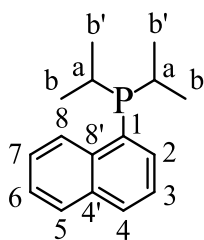
Diisopropyl(1-naphthyl)phosphine [91]: A solution of 1-bromonaphthalene (0.87 mL, 6.3 mmol) in THF (20 mL) was cooled to −78 °C. *n*-BuLi (4.1 mL, 1.6 M in *n*-hexane) was added dropwise. Thereafter, the mixture was allowed to reach r. t. for a short time and was then recooled to −78 °C. Diisopropylchlorophosphine (1 mL, 6.3 mmol) was added over 5 min. The reaction was stirred for 48 h at ambient conditions and the mixture was washed with nitrogen-saturated aqueous potassium carbonate solution for 10 min. The aqueous layer was extracted with diethylether (2 × 20 mL). The organic phases were combined, dried over potassium hydroxide, and the solvent removed under reduced pressure. The crude product was suspended in *n*-hexane. The liquid phase containing the product was separated from the precipitate by syringe. The solvent was removed in vacuum and product was recrystallized from 2 mL of *n*-hexane to give the product as a colorless solid. Yield: 165 mg, 0.68 mmol, 11%.

^{1}H-NMR (400 MHz, CD$_2$Cl$_2$), δ = 8.91 (1H, dd, *2-H*, $^3J_{HH}$ = 7.3 Hz, $^3J_{HP}$ = 6.9 Hz), 7.86 (2H, m, *5-*, *6-H*), 7.67 (1H, dd, *8-H*, $^3J_{HH}$ = 6.9 Hz, $^3J_{HH'}$ = 2.5 Hz), 7.51 (3H, m, *3-*, *4-*, *7-H*), 2.26 (2H, dd, *a-H*, $^3J_{HH}$ = 6.95 Hz, $^2J_{HP}$ = 1.1 Hz) 1.14 (6H, dd, *b-H*, $^3J_{HP}$ = 15.0 Hz, $^3J_{HH}$ = 6.95 Hz), 0.95 (6H, dd, *b'-H*, $^3J_{HP}$ = 11.9 Hz, $^3J_{HH}$ = 6.95 Hz) ppm.

^{13}C-NMR (100.6 MHz, CD$_2$Cl$_2$), δ = 138.9 (d, *8'-C* or *4'-C*, $^2J_{CP}$ = 22.2 Hz) 134.3 (d, *4'-C* or *8'-C*, $^3J_{CP}$ = 4.6 Hz), 133.6 (d, *1-C*, $^1J_{CP}$ = 21.0 Hz), 131.6 (s, *8-C*), 129.6 (s, *6-C*), 129.0 (d, *5-C*, $^4J_{CP}$ = 1.1 Hz), 127.4 (d, *2-C*, $^2J_{CP}$ = 30.9 Hz), 126.2 (d, *4-C*, $^4J_{CP}$ = 1.7 Hz), 126.1 (d, *3-C*, $^3J_{CP}$ = 2.2 Hz), 125.5 (s, *7-C*), 24.2 (2C, d, *a-C*, $^1J_{CP}$ = 12.4 Hz), 20.7 (6C, d, *b-C*, $^2J_{CP}$ = 18.4 Hz), 19.4 (6C, d, *b'-C*, $^2J_{CP}$ = 9.8 Hz) ppm.

^{31}P-NMR (162 MHz, CD$_2$Cl$_2$), δ = −8.55 (s, br) ppm.
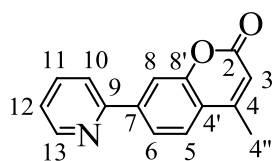
7-(Pyridin-2-yl)-4-methylcoumarin (L2): A mixture of 2-bromopyridine (0.6 mL, 6.08 mmol) in 20 mL of THF was cooled to −78 °C. *t*-BuLi (6.6 mL, 1.9 M in *n*-pentane) was added dropwise. The reaction mixture was stirred for 0.5 h and a solution of ZnCl$_2$ (0.83 g, 6.08 mmol) in THF (10 mL) was slowly added. The resulting mixture was stirred for 0.5 h at –78 °C and then allowed to reach r. t. After 0.5 h, the solvent was removed *in vacuo*. A solution of palladium(II)acetate (22.7 mg, 0.101 mmol) and diisopropyl(1-naphthyl)phosphine (29.8 mg, 0.122 mmol) in THF (5 mL) and a solution of 4-MCOTf (1.25 g, 4.05 mmol) in THF (20 mL) were added. The reaction was stirred for 21 h at 60 °C. The formation of a dark green suspension and a black precipitate of Pd(0) were observed. The solvent was removed and the remaining solid was suspended in DCM. This suspension was filtered over silica gel (3 cm). The filtrate was concentrated to 70 mL, washed with 50 mL of aqueous NH$_4$Cl solution,

and dried over MgSO$_4$. The solvent was removed under reduced pressure. Chromatographic purification on silica gel (ethyl acetate/petroleum ether 4:5) and recrystallization from dichloromethane layered with petroleum ether provided the product as a colorless solid. Yield: 210 mg, 0.89 mmol, 22%.

^{1}H-NMR (400 MHz, CDCl$_3$), δ = 8.62 (1H, dd, *13-H*, $^3J_{HH}$ = 4.80 Hz, $^4J_{HH}$ = 1.64 Hz), 7.86 (1H, dd, *6-H*, $^3J_{HH}$ = 8.28 Hz, $^4J_{HH}$ = 1.70 Hz), 7.81 (1H, d, *8-H*, $^4J_{HH}$ = 1.70 Hz), 7.69 (2H, m, *11-H, 10-H*), 7.55 (1H, d, *5-H*, $^3J_{HH}$ = 8.28 Hz), 7.20 (1H, ddd, *12-H*, $^3J_{HH}$ = 4.80 Hz, $^3J_{HH'}$ = 6.68 Hz, $^4J_{HH}$ = 1.64 Hz), 6.18 (1H, d, *3-H*, $^4J_{HH}$ = 1.25 Hz), 2.35 (3H, d, *4''-H*, $^4J_{HH}$ = 1.25 Hz) ppm.

^{13}C-NMR (100.6 MHz, CDCl$_3$), δ = 160.6 (s, *2-C*), 154.9 (s, *9-C*), 153.7 (s, *4-C*), 152.0 (s, *8'-C*), 149.8 (s, *13-C*), 142.5 (s, *7-C*), 137.0 (s, *11-C*), 124.9 (s, *5-C*), 123.1 (s, *12-C*), 122.5 (s, *6-C*), 120.7 (s, *10-C*), 120.1 (s, *4'-C*), 115.1 (s, *3-C*), 114.8 (s, *8-C*), 18.5 (s, *4''-C*) ppm.

IR (cm^{-1}): ν(C=O) = 1762 w, 1738 sh, 1712 vs, 1692 sh, 1678 sh, 1662 sh.

Analysis calculated for C$_{15}$H$_{11}$NO$_2$ × CDCl$_3$ (237.26): C, 73.63%; H, 4.57%; N, 5.70%; **found**: C, 73.69%; H, 4.67%; N, 5.86%.
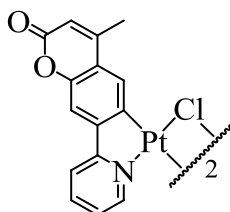
Bis-{μ-chloro-[4-methyl-7-(pyridin-2-yl)-*2H*-chromen-2-onato-*N'*,*C^6*)]-platinum(II)}, **[(7-PYC)Pt(μ-Cl)]$_2$:** 4-Methyl-7-(pyridin-2-yl)coumarin (78 mg, 0.33 mmol) and *cis*-[PtCl$_2$(dmso)$_2$] (129 mg,

0.3 mmol) were suspended in 6.6 mL of a water/2-methoxyethanol-mixture (1:3) and refluxed for 16 h at 80–90 °C. The obtained yellow suspension was allowed to reach r. t. Fourty milliliters of purified water were added and the mixture was cooled to 0 °C. A precipitate was filtered off, washed with ethanol (3 × 10 mL), and dried *in vacuo* to yield a yellow solid. Yield: 140 mg, 0.15 mmol, 99%.
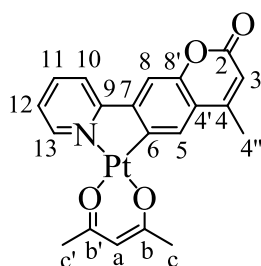
(4-Methyl-7-(pyridin-2-yl)-*2H*-chromen-2-onato-*N'*,*C^6*)(2,4-pentanedionato-*O,O*)-platinum(II) (2) : [(7-PYC)Pt(μ-Cl)]$_2$ (140 mg, 0.15 mmol), Na$_2$CO$_3$ (160 mg, 1.5 mmol) and acetylacetone (0.05 mL, 0.49 mmol) were suspended in 4.3 mL of 2-methoxyethanol. The resulting mixture was refluxed for 16 h at 90 °C and then allowed to reach r. t. An orange precipitate was isolated by decanting the solution and the crude product was extracted from that solid with DCM. The solvent was removed from the filtrate under reduced pressure. The crude product was washed with methanol

(1 × 20 mL) and n-pentane (2 × 20 mL) and dried *in vacuo*. Upon crystallization from dichloromethane layered with petroleum ether, the product was obtained as yellow needles. Yield: 102 mg, 0.19 mmol, 63%.

¹H-NMR (600 MHz, CD₂Cl₂), δ = 9.04 (1H, dd, *13-H*, $^3J_{HH}$ = 5.82 Hz, $^3J_{PtH}$ = 17.00 Hz), 7.92 (1H, dpt, *11-H*, $^3J_{HH}$ = 7.90 Hz, $^3J_{HH'}$ = 7.50 Hz, $^4J_{HH}$ = 1.40 Hz), 7.76 (1H, s, *5-H*, $^3J_{PtH}$ = 15.40 Hz), 7.72 (1H, d, *10-H*, $^3J_{HH}$ = 7.90 Hz), 7.42 (1H, s, *8-H*), 7.25 (1H, pt, *12-H*, $^3J_{HH}$ = 5.82 Hz, $^3J_{HH'}$ = 7.50 Hz), 6.24 (1H, d, *3-H*, $^4J_{HH}$ = 1.05 Hz), 5.54 (1H, s, *a-H*), 2.49 (3H, d, *4''-H*, $^4J_{HH}$ = 1.05 Hz), 2.03 (6H, 2 s, *c-H, c'-H*) ppm.

¹³C-NMR (151 MHz, CD₂Cl₂), δ = 186.8 (s, *b'-C*), 184.69 (s, *b-C*), 166.8 (s, *9-C*), 161.4 (s, *2-C*), 153.5 (s, *4-C*), 152.0 (s, *8'-C*), 148.8 (s, *7-C*), 148.1 (s, *13-C*), 139.2 (s, *11-C*), 132.7 (s, *6-C*), 125.7 (s, *5-C*), 123.4 (s, *12-C*), 120.8 (s, *4'-C*), 120.2 (s, *10-C*), 115.6 (s, *3-C*), 111.2 (s, *8-C*), 103.0 (s, *a-C*), 28.5 (s, *c'-C*), 27.4 (s, *c-C*), 19.2 (s, *4''-C*) ppm.

IR (cm⁻¹): ν(C=O) = 1778 w, 1715 vs, 1699 sh, 1682 sh, 1662 sh.

Analysis calculated for C₂₀H₁₇NO₄Pt (530.44): C, 45.29%; H, 3.23%; N, 2.64%; **found**: C, 45.12%; H, 3.23%; N, 2.87%.

Crystallographic data files have been deposited at the Cambridge Crystallographic Data Centre, 12, Union Road, Cambridge CB2 1EZ, [Fax: + 44 1223/336-033; E-mail deposit@ccdc.cam.ac.] and can be obtained free of charge at www.ccdc.cam.ac.uk/conts/retrieving.html. Deposition numbers are CCDC 1043115 (**1**) and 1043106 (**2**).

Acknowledgements

Author Contributions

Rainer Winter and Andrej Jackel devised this work and wrote the manuscript. Andrej Jackel performed the synthesis and characterization ligand **L1** and complexes **1** and **2**. He also performed the quantum chemical calculations with the help of Michael Linseis. Christoph Häge contributed the synthesis and characterization of ligand **L2** during an internship.

Appendix

Depictions of the ¹H and ¹³C{¹H} NMR spectra of all compounds; crystal and refinement data; full lists of bond parameters as well as additional packing diagrams of complexes **1** and **2**; graphical representations of IR spectra, exemplary cyclic voltammograms, and time-resolved traces of the emission spectra; overlays of calculated and experimental absorption spectra; tables with structure parameters for the optimized computed geometries of the complexes; energies and compositions of the FMOs; graphical representations of the crucial MOs of the complexes; and TD-DFT calculated transitions.

References

1. Brooks, W.J.; Babayan, V.; Lemansky, S.; Djurovich, P.I.; Tsyba, I.; Bau, R.; Thompson, M.E. Synthesis and Characterization of Phosphorescent Cyclometalated Platinum Complexes. *Inorg. Chem.* **2002**, *41*, 3055–3066.
2. Djurovich, P.I.; Murphy, D.; Thompson, M.E.; Hernandez, B.; Gao, R.; Hunt, P.L.; Selke, M. Cyclometalated iridium and platinum complexes as singlet oxygen photosensitizers: Quantum yields, quenching rates and correlation with electronic structures. *Dalton Trans.* **2007**, 3763–3770.
3. Bossi, A.; Rausch, A.F.; Leitl, M.J.; Czerwieniec, R.; Whited, M.T.; Djurovich, P.I.; Yersin, H.; Thompson, M.E. Photophysical Properties of Cyclometalated Pt(II) Complexes: Counterintuitive Blue Shift in Emission with an Expanded Ligand π System. *Inorg. Chem.* **2013**, *52*, 12403–12415.
4. Ionkin, A.S.; Marshall, W.J.; Wang, Y. Syntheses, Structural Characterization, and First Electroluminescent Properties of Mono-cyclometalated Platinum(II) Complexes with Greater than Classical π−π Stacking and Pt−Pt Distances. *Organometallics* **2005**, *24*, 619–627.
5. He, Z.; Wong, W.-Y.; Yu, X.; Kwok, H.-S.; Lin, Z. Phosphorescent Platinum(II) Complexes Derived from Multifunctional Chromophores: Synthesis, Structures, Photophysics, and Electroluminescence. *Inorg. Chem.* **2006**, *45*, 10922–10937.
6. Yin, B.; Niemeyer, F.; Williams, J.A.G.; Jiang, J.; Boucekkine, A.; Toupet, L.; Le Bozec, H.; Guerchais, V. Synthesis, Structure, and Photophysical Properties of Luminescent Platinum(II) Complexes Containing Cyclometalated 4-Styryl-Functionalized 2-Phenylpyridine Ligands. *Inorg. Chem.* **2006**, *45*, 8584–8596.
7. Chang, S.-Y.; Cheng, Y.-M.; Chi, Y.; Lin, Y.-C.; Jiang, C.-M.; Lee, G.-H.; Chou, P.-T. Emissive Pt(II) complexes bearing both cyclometalated ligand and 2-pyridyl hexafluoropropoxide ancillary chelate. *Dalton Trans.* **2008**, 6901–6911.
8. Kozhevnikov, D.N.; Kozhevnikov, V.N.; Ustinova, M.M.; Santoro, A.; Bruce, D.W.; Koenig, B.; Czerwieniec, R.; Fischer, T.; Zabel, M.; Yersin, H. Synthesis of Cyclometallated Platinum Complexes with Substituted Thienylpyridines and Detailed Characterization of Their Luminescence Properties. *Inorg. Chem.* **2009**, *48*, 4179–4189.
9. Wu, W.; Guo, H.; Ji, S.; Zhao, J. Long-Lived Room Temperature Deep-Red/Near-IR Emissive Intraligand Triplet Excited State (^{3}IL) of Naphthalimide in Cyclometalated Platinum(II) Complexes and Its Application in Upconversion. *Inorg. Chem.* **2011**, *50*, 11446–11460.
10. Tronnier, A.; Risler, A.; Langer, N.; Wagenblast, G.; Münster, I.; Strassner, T. A Phosphorescent C^C* Cyclometalated Platinum(II) Dibenzothiophene NHC Complex. *Organometallics* **2012**, *31*, 7447–7452.
11. Uesugi, H.; Tsukuda, T.; Takao, K.; Tsubomura, T. Highly emissive platinum(II) complexes bearing carbene and cyclometalated ligands. *Dalton Trans.* **2013**, *42*, 7396–7403.
12. Culham, S.; Lanoë, P.-H.; Whittle, V.L.; Durrant, M.C.; Williams, J.A.G.; Kozhevnikov, V.N. Highly Luminescent Dinuclear Platinum(II) Complexes Incorporating Bis-Cyclometallating Pyrazine-Based Ligands: A Versatile Approach to Efficient Red Phosphors. *Inorg. Chem.* **2013**, *52*, 10992–11003.

13. Moussa, J.; Cheminel, T.; Freeman, G.R.; Chamoreau, L.-M.; Williams, J.A.G.; Amouri, H. An unprecedented cyclometallated platinum(II) complex incorporating a phosphinine co-ligand: synthesis and photoluminescence behaviour. *Dalton Trans.* **2014**, *43*, 8162–8165.

14. Micksch, M.; Tenne, M.; Strassner, T. C^N-Cyclometalated Platinum(II) Complexes with Sterically Demanding 1,2-Diarylimidazole Ligands. *Organometallics* **2014**, *33*, 3464–3473.

15. Yu, J.; He, K.; Li, Y.; Tan, H.; Zhu, M.; Wang, Y.; Liu, Y.; Zhu, W.; Wu, H. A novel near-infrared-emitting cyclometalated platinum(II) complex with donor–acceptor–acceptor chromophores. *Dyes Pigments* **2014**, *107*, 146–152.

16. Liu, C.; Song, X.; Rao, X.; Xing, Y.; Wang, Z.; Zhao, J.; Qiu, J. Novel triphenylamine-based cyclometalated platinum(II) complexes for efficient luminescent oxygen sensing. *Dyes Pigm.* **2014**, *101*, 85–92.

17. Wu, W.; Wu, W.; Ji, S.; Guo, H.; Song, P.; Han, K.; Chi, L.; Shao, J.; Zhao, J. Tuning the emission properties of cyclometalated platinum(II) complexes by intramolecular electron-sink/arylethynylated ligands and its application for enhanced luminescent oxygen sensing. *J. Mater. Chem.* **2010**, *20*, 9775–9786.

18. Lai, S.-W.; Che, C.-M. Luminescent Cyclometalated Diimine Platinum(II) Complexes: Photophysical Studies and Applications *Top. Curr. Chem.* **2004**, *241*, 27–63.

19. Williams, J.A.G. Photochemistry and Photophysics of Coordination Compounds: Platinum. *Top. Curr. Chem.* **2007**, *281*, 205–268.

20. Thompson, M.E.; Djurovich, P.I.; Barlow, S.; Marder, S.R. Organometallic Complexes for optoelectronic applications. In *Comprehensive Organometallic Chemistry*; O'Hare, D., Ed.; Elsevier: Oxford, UK, 2007; Volume 12; pp. 101–194.

21. Chi, Y.; Chou, P.-T. Transition-metal phosphors with cyclometalating ligands: Fundamentals and applications. *Chem. Soc. Rev.* **2010**, *39*, 638–655.

22. Wong, W.-Y.; Ho, C.-L. Heavy metal organometallic electrophosphors derived from multi-component chromophores. *Coord. Chem. Rev.* **2009**, *253*, 1709–1758.

23. Yersin, H.; Rausch, A.F.; Czerwieniec, R.; Hofbeck, T.; Fischer, T. The triplet state of organo-transition metal compounds. Triplet harvesting and singlet harvesting for efficient OLEDs. *Coord. Chem. Rev.* **2011**, *255*, 2622–2652.

24. Bronner, C.; Baudron, S.A.; Hosseini, M.W.; Strassert, C.A.; Guenet, A.; de Cola, L. Dipyrrin based luminescent cyclometallated palladium and platinum complexes. *Dalton Trans.* **2010**, *39*, 180–184.

25. Bronner, C.; Veiga, M.; Guenet, A.; de Cola, L.; Hosseini, M.W.; Strassert, C.A.; Baudron, S.A. Excited State Properties and Energy Transfer within Dipyrrin-Based Binuclear Iridium/Platinum Dyads: The Effect of ortho-Methylation on the Spacer. *Chem. Eur. J.* **2012**, *18*, 4041–4050.

26. Naziruddin, A.R.; Galstyan, A.; Iordache, A.; Daniliuc, C.G.; Strassert, C.A.; de Cola, L. Bidentate NHC^pyrozolate ligands in luminescent platinum(II) complexes. *Dalton Trans.* **2015**, doi:10.1039/C1034DT03651D.

27. Zhou, G.-J.; Wang, Q.; Wong, W.-Y.; Ma, D.; Wang, L.; Lin, Z. A versatile color tuning strategy for iridium(III) and platinum(II) electrophosphors by shifting the charge-transfer states with an electron-deficient core. *J. Mater. Chem.* **2009**, *19*, 1872–1883.

28. Tam, A.Y.-Y.; Tsang, D.P.-K.; Chan, M.-Y.; Zhu, N.; Yam, V.W.-W. A luminescent cyclometalated platinum(II) complex and its green organic light emitting device with high device performance. *Chem. Commun.* **2011**, *47*, 3383–3385.

29. Wu, W.; Cheng, C.; Wu, W.; Guo, H.; Ji, S.; Song, P.; Han, K.; Zhao, J.; Zhang, X.; Wu, Y.; Du, G. Tuning the Emission Colour of Triphenylamine-Capped Cyclometallated Platinum(II) Complexes and Their Application in Luminescent Oxygen Sensing and Organic Light-Emitting Diodes. *Eur. J. Inorg. Chem.* **2010**, *2010*, 4683–4696.

30. Wu, W.; Wu, W.; Ji, S.; Guo, H.; Zhao, J. Accessing the long-lived emissive ^{3}IL triplet excited states of coumarin fluorophores by direct cyclometallation and its application for oxygen sensing and upconversion. *Dalton Trans.* **2011**, *40*, 5953–5963.

31. Pevny, F.; Zabel, M.; Winter, R.F.; Rausch, A.F.; Yersin, H.; Tuczek, F.; Záliš, S. Improvement of (bipy)Pt(XR)$_2$ (X = O, S) type photosensitizers by covalent dye attachment. *Chem. Commun.* **2011**, 6302–6304.

32. Wu, W.; Ji, S.; Wu, W.; Shao, J.; Guo, H.; James, T.D.; Zhao, J. Ruthenium(II)–Polyimine–Coumarin Light-Harvesting Molecular Arrays: Design Rationale and Application for Triplet–Triplet-Annihilation-Based Upconversion. *Chem. Eur. J.* **2012**, *18*, 4953–4964.

33. Guo, H.; Qin, H.; Chen, H.; Sun, H.; Zhao, J. Phenylacetylide ligand mediated tuning of visible-light absorption, room temperature phosphorescence lifetime and triplet–triplet annihilation based up-conversion of a diimine Pt(II) bisacetylide complex. *Dyes Pigments* **2013**, *99*, 908–915.

34. Sun, H.; Guo, H.; Wu, W.; Liu, X.; Zhao, J. Coumarin phosphorescence observed with N^NPt(II) bisacetylide complex and its applications for luminescent oxygen sensing and triplet-triplet-annihilation based upconversion. *Dalton Trans.* **2011**, *40*, 7834–7841.

35. Ulbricht, C.; Rehmann, N.; Holder, E.; Hertel, D.; Meerholz, K.; Schubert, U.S. Synthesis and Characterization of Oxetane-Functionalized Phosphorescent Ir(III)-Complexes. *Macromol. Chem. Phys.* **2009**, *210*, 531–541.

36. Geist, F.; Jackel, A.; Winter, R.F. Dual ligand-based fluorescence and phosphorescence emission at room temperature from platinum thioxanthonyl complexes. *Dalton Trans.* **2015**, *44*, 3974–3987.

37. Yu, T.; Yang, S.; Zhao, Y.; Zhang, H.; Fan, D.; Han, X.; Liu, Z. Synthesis, crystal structure and photoluminescent property of an iridium complex with coumarin derivative ligand. *Inorg. Chim. Acta* **2011**, *379*, 171–174.

38. Yu, T.; Yang, S.; Zhao, Y.; Zhang, H.; Han, X.; Fan, D.; Qiu, Y.; Chen, L. Synthesis, crystal structures and fluorescence properties of 3-(2-pyridyl)coumarin derivatives. *J. Photochem. Photobiol. A* **2010**, *214*, 92–99.

39. Du, L.; Li, M.; Zheng, S.; Wang, B. Rational design of a fluorescent hydrogen peroxide probe based on the umbelliferone fluorophore. *Tetrahedron Lett.* **2008**, *49*, 3045–3048.

40. Shimizu, H.; Manabe, K. Negishi coupling strategy of a repetitive two-step method for oligoarene synthesis. *Tetrahedron Lett.* **2006**, *47*, 5927–5931.

41. Wolfe, J.P.; Buchwald, S.L. A Highly Active Catalyst for the Room-Temperature Amination and Suzuki Coupling of Aryl Chlorides. *Angew. Chem. Int. Ed. Engl.* **1999**, *38*, 2413–2416.

42. Cockburn, B.N.; Howe, D.V.; Keating, T.; Johnson, B.F.G.; Lewis, J. Reactivity of co-ordinated ligands. Part XV. Formation of complexes containing Group V donor atoms and metal-carbon σ-bonds. *Dalton Trans.* **1973**, 404–410.

43. Godbert, N.; Pugliese, T.; Aiello, I.; Bellusci, A.; Crispini, A.; Ghedini, M. Efficient, Ultrafast, Microwave-Assisted Syntheses of Cycloplatinated Complexes. *Eur. J. Inorg. Chem.* **2007**, *2007*, 5105–5111.

44. Mdleleni, M.M.; Bridgewater, J.S.; Watts, R.J.; Ford, P.C. Synthesis, Structure, and Spectroscopic Properties of Ortho-Metalated Platinum(II) Complexes. *Inorg. Chem.* **1995**, *34*, 2334–2342.

45. Ghedini, M.; Pucci, D.; Crispini, A.; Barberio, G. Oxidative Addition to Cyclometalated Azobenzene Platinum(II) Complexes: A Route to Octahedral Liquid Crystalline Materials. *Organometallics* **1999**, *18*, 2116–2124.

46. Li, K.; Cheng, G.; Ma, C.; Guan, X.; Kwok, W.-M.; Chen, Y.; Lu, W.; Che, C.-M. Light-emitting platinum(II) complexes supported by tetradentate dianionic bis(*N*-heterocyclic carbene) ligands: towards robust blue electrophosphors. *Chem. Sci.* **2013**, *4*, 2630–2644.

47. Wong, W.-W.; He, Z.; So, S.-K.; Tong, K.-L.; Lin, Z. A Multifunctional Platinum-Based Triplet Emitter for OLED Applications. *Organometallics* **2005**, *24*, 4079–4082.

48. Lai, S.-W.; Chan, M.C.-W.; Cheung, T.-C.; Peng, S.-M.; Che, C.-M. Probing d^8–d^8 Interactions in Luminescent Mono- and Binuclear Cyclometalated Platinum(II) Complexes of 6-Phenyl-2,2'-bipyridines. *Inorg. Chem.* **1999**, *38*, 4046–4055.

49. Lu, W.; Chan, M.C.W.; Zhu, N.; Che, C.-M.; Li, C.; Hui, Z. Structural and Spectroscopic Studies on Pt···Pt and π−π Interactions in Luminescent Multinuclear Cyclometalated Platinum(II) Homologues Tethered by Oligophosphine Auxiliaries. *J. Am. Chem. Soc.* **2004**, *126*, 7639–7651.

50. Kui, S.C.F.; Chui, S.S.-Y.; Che, C.-M.; Zhu, N. Structures, Photoluminescence, and Reversible Vapoluminescence Properties of Neutral Platinum(II) Complexes Containing Extended π-Conjugated Cyclometalated Ligands. *J. Am. Chem. Soc.* **2006**, *128*, 8297–8309.

51. Kui, S.C.F.; Sham, I.H.T.; Cheung, C.C.C.; Ma, C.-W.; Yan, B.; Zhu, N.; Che, C.-M.; Fu, W.-F. Platinum(II) Complexes with π-Conjugated, Naphthyl-Substituted, Cyclometalated Ligands (RC^N^N): Structures and Photo- and Electroluminescence. *Chem. Eur. J.* **2007**, *7*, 417–435.

52. Miller, J.S.; Epstein, A.J. One-Dimensional Inorganic Complexes. In *Progress in Inorganic Chemistry*; John Wiley & Sons, Inc.: Weinheim, Germany, 1976; pp. 1–151.

53. Sun, Y.; Ye, K.; Zhang, H.; Zhang, J.; Zhao, L.; Li, B.; Yang, G.; Yang, B.; Wang, Y.; Lai, S.-W.; Che, C.-M. Luminescent One-Dimensional Nanoscale Materials with PtII···PtII Interactions. *Angew. Chem. Int. Ed.* **2006**, *45*, 5610–5613.

54. Rodionova, O.A.; Puzyk, M.V.; Balashev, K.P. Effect of cyclopalladation on the spectroscopic properties of a coumarin dye. *Opt. Spectrosc.* **2008**, *105*, 62–66.

55. Kaim, W.; Ernst, S.; Kohlmann, S. Farbige Komplexe: das Charge-Transfer Phänomen. *Chem. Uns. Zeit* **1987**, *21*, 50–58.

56. Krejcik, M.; Danek, M.; Hartl, F. Simple construction of an infrared optically transparent thin-layer cell: Applications to the redox reactions of ferrocene, $Mn_2(CO)_{10}$ and $Mn(CO)_3(3,5$-di-t-butyl-catecholate)$^-$. *J. Electroanal. Chem.* **1991**, *317*, 179–187.

57. Rachford, A.A.; Goeb, S.; Castellano, F.N. Accessing the Triplet Excited State in Perylenediimides. *J. Am. Chem. Soc.* **2008**, *130*, 2766–2767.

58. Kim, K.-Y.; Liu, S.; Köse, M.E.; Schanze, K.S. Photophysics of Platinum-Acetylide Substituted Hexa-peri-hexabenzacoronenes. *Inorg. Chem.* **2006**, *45*, 2509–2519.

59. Liu, L.; Huang, D.; Draper, S.M.; Yi, X.; Wu, W.; Zhao, J. Visible light-harvesting trans bis(alkylphosphine) platinum(II)-alkynyl complexes showing long-lived triplet excited states as triplet photosensitizers for triplet-triplet annihilation upconversion. *Dalton Trans.* **2013**, *42*, 10694–10706.

60. Guo, H.; Muro-Small, M.L.; Ji, S.; Zhao, J.; Castellano, F.N. Naphthalimide Phosphorescence Finally Exposed in a Platinum(II) Diimine Complex. *Inorg. Chem.* **2010**, *49*, 6802–6804.

61. Wu, W.; Zhao, J.; Sun, J.; Huang, L.; Yi, X. Red-light excitable fluorescent platinum(II) bis(aryleneethynylene) bis(trialkylphosphine) complexes showing long-lived triplet excited states as triplet photosensitizers for triplet-triplet annihilation upconversion. *J. Mater. Chem. C* **2013**, *1*, 705–716.

62. Nguyen, M.-H.; Yip, J.H.K. Platinum-Conjugated Homo- and Heterobichromophoric Complexes of Tetracene and Pentacene. *Organometallics* **2012**, *31*, 7522–7531.

63. Nguyen, M.-H.; Nguyen, V.H.; Yip, J.H.K. Sequence-Specific Synthesis of Platinum-Conjugated Trichromophoric Energy Cascades of Anthracene, Tetracene, and Pentacene and Fluorescent "Black Chromophores". *Organometallics* **2013**, *32*, 7283–7291.

64. Tanaka, Y.; Wong, K.M.-C.; Yam, V.W.-W. Platinum-Based Phosphorescent Double-Decker Tweezers: A Strategy for Extended Heterologous Metal–Metal Interactions. *Angew. Chem, Int. Ed.* **2013**, *52*, 14117–14120.

65. Chan, A.K.-W.; Lam, E.S.-H.; Tam, A.Y.-Y.; Tsang, D.P.-K.; Lam, W.H.; Chan, M.-Y.; Wong, W.-T.; Yam, V.W.-W. Synthesis and Characterization of Luminescent Cyclometalated Platinum(II) Complexes of 1,3-Bis-Hetero-Azolylbenzenes with Tunable Color for Applications in Organic Light-Emitting Devices through Extension of π Conjugation by Variation of the Heteroatom. *Chem. Eur. J.* **2013**, *19*, 13910–13924.

66. Leung, S.Y.-L.; Lam, E.S.-H.; Lam, W.H.; Wong, K.M.-C.; Wong, W.-T.; Yam, V.W.-W. Luminescent Cyclometalated Alkynylplatinum(II) Complexes with a Tridentate Pyridine-Based N-Heterocyclic Carbene Ligand: Synthesis, Characterization, Electrochemistry, Photophysics, and Computational Studies. *Chem. Eur. J.* **2013**, *19*, 10360–10369.

67. Bennett, M.A.; Bhargava, S.K.; Cheng, E.C.-C.; Lam, W.H.; Lee, T.K.-M.; Privér, S.H.; Wagler, J.; Willis, A.C.; Yam, V.W.-W. Unprecedented Near-Infrared (NIR) Emission in Diplatinum(III) (d^7-d^7) Complexes at Room Temperature. *J. Am. Chem. Soc.* **2010**, *132*, 7094–7103.

68. Pomestchenko, I.E.; Luman, C.R.; Hissler, M.; Ziessel, R.; Castellano, F.N. Room Temperature Phosphorescence from a Platinum(II) Diimine Bis(pyrenylacetylide) Complex. *Inorg. Chem.* **2003**, *42*, 1394–1396.

69. Kozhevnikov, D.N.; Kozhevnikov, V.N.; Shafikov, M.Z.; Prokhorov, A.M.; Bruce, D.W.; Gareth Williams, J.A. Phosphorescence *vs.* Fluorescence in Cyclometalated Platinum(II) and Iridium(III) Complexes of (Oligo)thienylpyridines. *Inorg. Chem.* **2011**, *50*, 3804–3815.

70. Liu, Y.; Guo, H.; Zhao, J. Ratiometric luminescent molecular oxygen sensors based on uni-luminophores of C^N Pt(II)(acac) complexes that show intense visible-light absorption and balanced fluorescence/phosphorescence dual emission. *Chem. Commun.* **2011**, *47*, 11471–11473.

71. Chia, Y.Y.; Tay, M.G. An insight into fluorescent transition metal complexes. *Dalton Trans.* **2014**, *43*, 13159–13168.

72. Kukushkin, V.Y.; Pombeiro, A.J.L. Compounds of general interest. Dimethylsulfoxide complexes of Pt(II): K[PtCl$_3$(Me$_2$SO)], cis-[PtCl$_2$L(Me$_2$SO)] (L = Me$_2$SO, MeCN), [PtCl(μ-Cl)(Me$_2$SO)]$_2$, and [Pt(Me$_2$SO)$_4$](CF$_3$SO$_3$)$_2$ *Inorg. Synth.* **2002**, *33*, 192.

73. Sheldrick, G.M. *SHELX-97*; Program for Crystal Structure Solution and Refinement; University of Göttingen: Göttingen, Germany, 1997.

74. Frisch, M.J.; Trucks, G.; Schlegel, H.B.; Scuseria, G.E.; Robb, M.A.; Cheeseman, J.R.; Scalmani, G.; Barone, V.; Mennucci, B.; Petersson, G.A.; *et al. Gaussian 09*, Revision C.01; Gaussian Inc.: Wallingford, CT, 2009.

75. Gunnarsson, O.; Lundqvist, B.I. Exchange and correlation in atoms, molecules, and solids by the spin-density-functional formalism *Phys. Rev. B* **1976**, *13*, 4274.

76. Dolg, M.; Stoll, H.; Preuss, H. Energy-adjusted *ab initio* pseudopotentials for the rare earth elements *J. Chem. Phys.* **1989**, *90*, 1730–1734.

77. Küchle, W.; Dolg, M.; Stoll, H.; Preuss, H. Energy-adjusted pseudopotentials for the actinides. Parameter sets and test calculations for thorium and thorium monoxide. *J. Chem. Phys.* **1994**, *100*, 7535–7532.

78. Andrae, D.; Haeussermann, U.; Dolg, M.; Stoll, H.; Preuss, H. Energy-adjusted *ab initio* pseudopotentials for the second and third row transition elements. *Theor. Chim. Acta* **1990**, *77*, 123–141.

79. Hariharan, P.H.; Pople, J.A. The Influence of Polarization Functions on Molecular Orbital Hydrogenation Energies. *Theor. Chim. Acta* **1973**, *28*, 213–222.

80. Perdew, J.P.; Burke, K.; Enzerhof, M. Generalized Gradient Approximation Made Simple. *Phys. Rev. Lett.* **1996**, *77*, 3865–3868.

81. Adamo, C.; Barone, V. Toward reliable density functional methods without adjustable parameters: The PBE0 model. *J. Chem. Phys.* **1999**, *110*, 6158–6170.

82. Becke, A.D. Density-functional thermochemistry. III. The role of exact exchange. *J. Chem. Phys.* **1993**, *98*, 5648–5652.

83. Stephens, P.J.; Devlin, F.J.; Chabalowski, C.F.; Frisch, M.J. *Ab Initio* Calculation of Vibrational Absorption and Circular Dichroism Spectra Using Density Functional Force Fields. *J. Phys. Chem.* **1994**, *98*, 11623–11627.

84. Cancés, E.; Menucci, B.; Tomasi, J. A new integral equation formalism for the polarizable continuum model: Theoretical background and applications to isotropic and anisotropic dielectrics. *J. Chem. Phys.* **1997**, *107*, 3032–3041.

85. Mennucci, B.; Tomasi, J. Continuum solvation models: A new approach to the problem of solute's charge distribution and cavity boundaries *J. Chem. Phys.* **1997**, *106*, 5151–5158.

86. Cossi, M.; Rega, N.; Scalmani, G.; Barone, V. Energies, structures, and electronic properties of molecules in solution with the C-PCM solvation model. *J. Comput. Chem.* **2003**, *24*, 669–681.

87. Scalamani, G.; Frisch, M.J. Continuous surface charge polarizable continuum models of solvation. I. General formalism. *J. Chem. Phys.* **2010**, *132*, 114110–114124.

88. Runge, E.; Gross, E.K.U. Density-Functional Theory for Time-Dependent Systems. *Phys. Rev. Lett.* **1984**, *52*, 997–1000.

89. O'Boyle, N.M.; Tenderholt, A.L.; Langner, K.M. cclib: A library for package-independent computational chemistry algorithms. *J. Comput. Chem.* **2008**, *29*, 839–845.

90. Keith, T.; Millam, J. *GaussView*, Version 3; Semichem Inc.: Shawnee Mission KS, 2009.

91. Hu, R.-B.; Zhang, H.; Zhang, X.-Y.; Yang, S.-D. Palladium-catalyzed $P(O)R_2$ directed C-H arylation to synthesize electron-rich polyaromatic monophosphorus ligands. *Chem. Commun.* **2014**, *50*, 2193–2195.